Insights into the limitations to vibrational excitation of CO_2 : validation of a kinetic model with pulsed glow discharge experiments

Insights into the limitations to vibrational excitation of CO_2: validation of a kinetic model with pulsed glow discharge experiments

Omar Biondo[1,2], Chloé Fromentin[3], Tiago Silva[3], Vasco Guerra[3], Gerard van Rooij[2,4], Annemie Bogaerts[1]

[1]Research Group PLASMANT, Department of Chemistry, University of Antwerp, Universiteitsplein 1, Wilrijk B-2610, Belgium

[2]DIFFER, 5612AJ Eindhoven, The Netherlands

[3]Instituto de Plasmas e Fusão Nuclear, Instituto Superior Técnico, Universidade de Lisboa, 1049-001 Lisboa, Portugal

[4]Faculty of Science and Engineering, Maastricht University, 6229 GS Maastricht, The Netherlands

E-mail: Omar.Biondo@uantwerpen.be

Abstract

Vibrational excitation represents an efficient channel to drive the dissociation of CO_2 in a non-thermal plasma. Its viability is investigated in low-pressure pulsed discharges, with the intention of selectively exciting the asymmetric stretching mode, leading to stepwise excitation up to the dissociation limit of the molecule. Gas heating is crucial for the attainability of this process,

since the efficiency of vibration-translation relaxation strongly depends on temperature, creating a feedback mechanism that can ultimately thermalize the discharge. Indeed, recent experiments demonstrated that the timeframe of vibration-translation non-equilibrium is limited to a few milliseconds at ca. 6 mbar, and shrinks to the μs-scale at 100 mbar. With the aim of backtracking the origin of gas heating in pure CO_2 plasma, we perform a kinetic study to describe the energy transfers under typical non-thermal plasma conditions. The validation of our kinetic scheme with pulsed glow discharge experiments enables to depict the gas heating dynamics. In particular, we pinpoint the role of vibration-vibration-translation relaxation in redistributing the energy from asymmetric to symmetric levels of CO_2, and the importance of collisional quenching of CO_2 electronic states in triggering the heating feedback mechanism in the sub-millisecond scale. This latter finding represents a novelty for the modelling of low-pressure pulsed discharges and we suggest that more attention should be paid to it in future studies. Additionally, O atoms convert vibrational energy into heat, speeding up the feedback loop. The efficiency of these heating pathways, even at relatively low gas temperature and pressure, underpins the lifetime of vibration-translation non-equilibrium and suggests a redefinition of the optimal conditions to exploit the “ladder-climbing” mechanism in CO_2 discharges.

Keywords: Vibrational excitation, CO_2 conversion, gas heating, non-thermal plasma, glow discharges, pulsed discharges.

1. Introduction

Carbon dioxide emissions are considered the origin of climate change. Therefore, their reduction is highly desirable and the society is put under particular pressure to find a solution before long. Model simulations suggested that CO_2 increase in the atmosphere might have a direct impact on Northern Hemisphere summer temperature, heat stress, and tropical precipitation extremes [1]. It has been pointed out that temperature targets alone are insufficient to limit the risks associated with anthropogenic emissions [2,3]. Indeed, the existing fossil-fuel energy infrastructure will emit about 658 Gt CO_2 by 2050, if operated in a "business as usual" way, which will lead the global temperature increase to exceed the 1.5 °C target [4]. Around 54 % of these emissions comes from the power sector, which puts more pressure on the need of decarbonizing the power production. Under this pressure, the development of alternatives to the use of fossil carbon has become a priority in many countries. Renewable energy is expected to contribute to half of the growth in global energy supplies and become the largest source of power by 2040 [5]. As a drawback, renewable energy sources have intermittent production rates and are inherently not well balanced with the fluctuations in the electricity demand. More specific, conventional fossil-based sources are still needed to supplement periods of shortage (e.g. reduced daylight during winter, absence of wind, drought) in electricity demand. On the other hand, when the production exceeds the demand, the generation of renewable energy cannot be fully exploited and has to be lowered, causing economical losses [6]. Therefore, the development of technologies able to simultaneously reduce CO_2 emissions and store the excess of renewable energy into chemical bonds of fuels is of vital importance.

To this end, plasma technology stands out for (i) its high process versatility, allowing performing different types of reactions in combination with CO_2 splitting (e.g. dry reforming of methane, CO_2 hydrogenation or CO_2 methanation); (ii) the intrinsic low investment and operating costs

(depending on the type of plasma reactor); (iii) the rare earth metal-free operation; (iv) its scalability; and (v) being easily combined with various kinds of renewable energy [7]. In the past decade, many different plasma sources have been investigated, with the aim of finding the optimal conditions for an energy-efficient conversion, with a combination of experiments and computational efforts. For instance, extensive research was carried out on CO_2 dissociation in low-power glow discharges [8–10] and in high power microwave discharges [11–14]. These two types of discharges operate in regimes associated with different dominant mechanisms for CO_2 splitting. In fact, the former are low-excitation and non-equilibrium discharges (at least when operated at low pressure), whereas the latter can be described as “warm” plasmas, where the gas () and vibrational () temperature are almost in equilibrium with each other, and are typically not much lower than the electron temperature (T_e) (i.e.) [12,15,16]. For “warm” plasmas, with T_g = 3000-4000 K (or more in case of contraction [15]), the conversion is mostly thermally-driven [17]. Under these conditions, high conversion rates and energy efficiencies of up to 80% and 50% (close to the theoretical efficiency limit 52%, with no CO losses in back-reactions [18]), respectively, were achieved [19,20]. Nevertheless, the thermal pathway for CO_2 cannot explain alone the energy efficiencies higher than 80% reported for the splitting of CO_2 in the past [21,22]. Recently, van de Steeg *et al.* [23] proposed a redefinition of the thermal limit to 70% for the energy efficiency, proving that the combination of fast transport and high energy deposition in the core can result in a local chemical non-equilibrium, where additional CO_2 dissociation through the O-CO_2 association might occur. However, a 70% energy efficiency is still lower than the previous experimental observations [21,22].

Alternatively, it has been hypothesized that the stepwise vibrational excitation of the asymmetric stretching mode of CO_2 () up to the dissociation limit, also called “ladder-climbing” mechanism

and similar to vibrational pooling [24,25], can be the key for a highly efficient CO_2 conversion into CO [26]. This is due to the minimum amount of energy (ca. 5.5 eV) to break the C=O bond at the bond enthalpy along the axes of asymmetric vibrations [27,28]. The negative anharmonicity of (i.e. the level spacing decreases for higher levels) promotes the overpopulation of the higher levels through vibration-vibration (V-V) collisions, eventually leading to splitting of the molecule [29,30]. However, T_g should be maintained low in order to avoid vibration-translation relaxation and conserve an effective "ladder-climbing" [26].

As previously mentioned, low-power glow discharges are typically grouped under the family of low-temperature plasmas (LTPs), which, by definition, are characterized by low T_g and a certain degree of vibration-translation (V-T) non-equilibrium. Therefore, this category represents a good candidate to explore the optimal conditions for a consistent vibrational excitation. Here, quenching of vibrational quanta to heat (V-T relaxation) constitutes an important pathway for vibrational energy loss and, consequently, gas heating [29]. The onset of V-T relaxation triggers a feedback loop between gas heating and vibrational deactivation because the rate coefficient of V-T relaxation increases with T_g. This eventually guides the discharge towards a V-T equilibrium, making the exploitation of the "ladder-climbing" mechanism very challenging [18,31]. In order to stop such a loop mechanism and limit T_g during the operations, power pulsing has been brought to attention as a convenient approach to attain high energy efficiency by modulating the pulse and inter-pulse duration [32]. Moreover, power pulsing enables the study of the plasma kinetics during the onset of the discharge, providing useful insights into the underlying mechanisms for vibrational excitation and relaxation and their role into the gas heating dynamics [8,9,14,33,34] and the recombination of O atoms to O_2 that can affect CO_2 conversion [35]. Therefore, pulsed low-power glow discharges form an ideal testbed for

validation of kinetic models. In fact, glow discharges are an extremely useful instrument for studying the plasma kinetics, providing a simple geometry that can be safely approximated to a plug flow reactor (PFR) [36] and allowing for the application of many *in-situ* diagnostics (e.g. Fourier Transform Infrared (FTIR) spectroscopy [8], Raman scattering [37], Optical Emission Spectroscopy (OES) [38] and actinometry [39]).

With this in mind, we chose to verify our kinetic scheme for vibrational excitation and heating dynamics in CO_2 low-temperature plasmas with the experiments presented by Klarenaar *et al.* [8]. This set of experiments was already applied to unveil the relevant reactions for vibrational excitation, during the active phase of the discharge [34], and relaxation, in the afterglow [9]. These two contributions opened the possibility of using a state-to-state approach to benchmark the validity of a multi-temperature description of CO_2 plasmas for capturing some essential features of non-equilibrium phenomena, as previously done for N_2 [40], with reduced computational effort. For instance, Kosareva *et al*. [41] demonstrated that the state-to-state approach can be substituted by the multi-temperature approach for the problem of spatially homogeneous relaxation in non-equilibrium CO_2 flows, without sacrificing the accuracy of the results. The multi-temperature description consisted of up to 4 different temperatures, namely T_g, and the vibrational temperatures of the symmetric stretching (T_1), bending (T_2) and asymmetric (T_3) levels [41]. Alternatively, symmetric and bending modes can be described by T_{12} thanks to the Fermi resonance between their levels (more details in section 2), reducing the description to a three-temperature model.

Despite T_g is a key parameter determining the efficiency of vibrational energy exchanges and, more in general, a macroscopic descriptor of plasmas, only a few modelling studies featured its self-consistent calculation for CO_2 discharges. This means that in most cases we can only

estimate the degree of vibrational excitation when we know T_g from the experiments. The possibility of calculating T_g from the discharge parameters (i.e. power and volume) enables an appropriate understanding of the gas heating and, ultimately, a better definition of the optimal discharge conditions to harness vibration-translation non-equilibrium. In the context of N_2 and N_2-O_2 mixtures, Pintassilgo and Guerra [42] studied the energy transfer to gas heating with a Zero-Dimensional (0D) kinetic model. In particular, the authors showed that the energy transferred to heat increases with O_2 addition to N_2, with a maximum at 20%, in line with experimental observations. More recently, Kelly *et al*. [43] inferred the plasma dynamics in a N_2 pulsed MW discharge by a combination of 0D modelling and experiments. Specifically, their study elucidated the role of gas heating in inducing thermal-ionization instabilities, which are believed to drive the discharge volume contraction with rising gas pressure. Other contributions on the modelling of these mixtures can be found in the review by Popov and Starikovskaia [44]. For CO_2 plasma discharges, Silva *et al*. [45] modelled the afterglow of a pulsed glow discharge with a self-consistent calculation of T_g, providing a very good agreement with the experimental T_g evolution. Their work proved that the gas heating dynamics in the post-discharge region can be accurately described by V-T and V-V relaxation. Their observation finds additional confirmation in our calculations. However, the energy transfer scheme depicted by their heating analysis may not be sufficiently descriptive for the active part of the discharge.

Recently, Pokrovskiy *et al.* [46] studied the relevant mechanisms underlying the onset of gas heating in a nanosecond capillary discharge at 19-20 mbar. These types of discharges feature E/N typically larger than pulsed glow discharges (i.e. 150-250 Td), promoting the direct electron-impact dissociation over the “ladder-climbing” mechanism. Under these conditions the well-known phenomenon of the fast gas heating (FGH) [47] dominates the heating dynamics

during the pulse on-time [46]. FGH is described as an abrupt increase in T_g occurring in LTPs due to fast transfer of energy from electronic to translational degrees of freedom [47]. This mechanism can consume an important fraction of the energy deposited by the electrons onto molecules, limiting the performance and efficiency of the reactor. The mechanism of FGH, which occurs at the sub-microsecond timescale, was traced back to the quenching reactions of $CO(a^3\Pi)$, $O(^1S)$ and $O(^1D)$ excited species, which are products of the direct electron-impact dissociation of CO_2 [46]. This heating channel is faster than typical V-T and V-V relaxation [44], which cannot fully describe the heating dynamics. Indeed, van de Steeg *et al.* [14] showed that V-T relaxation makes up only ca. 50% of the total heating rate in a pulsed microwave (MW) discharge (pulse time = 200 μs, p = 25 mbar). Under these conditions, the characteristic V-T relaxation time can be estimated to be about 0.15 ms at 300 K [48], thus other heating pathways need to be taken into account to explain the T_g evolution. Similar conclusions can be drawn for the pulsed glow discharge case, i.e. gas heating onsets at t < 0.1 ms, before the maximum vibrational excitation is reached (0.9 ms) [8].

In this perspective, we developed a 0D kinetic model to reproduce the temperature (T_g, T_{12} and T_3) evolution measured by [8] and verify our new kinetic scheme, which includes a detailed description of the vibrational chemistry of CO_2, along with the electronic excitation and relaxation of different species. We constructed the kinetic scheme starting from the preceding modelling efforts of both the research groups (N-PRiME [9,33,34] and PLASMANT [29,49–51]), following a procedure established within the framework of this collaboration. In this work, we focused on the modelling of the “single-pulse” measurements [8], where the dissociation degree throughout the pulse is negligible and no dissociation products are left in the subsequent pulse. In this way, we could study the CO_2 vibrational and electronic kinetics and their role into

the gas heating dynamics, decoupling it from the influence of dissociation products. The inclusion of the collisional quenching of CO_2 electronic states represents a novelty in the modelling of low-pressure pulsed discharges that deserves more attention in the study of the energy transfers in CO_2 plasmas. Upon the verification of the kinetic scheme proposed, here we demonstrate the importance of the relaxation of electronically excited molecules besides vibrational deactivation, which we could bring to light via a self-consistent calculation of T_g.

2. The CO_2 vibrational levels

The CO_2 molecule has vibrational normal modes: the v_1 symmetric stretching, the doubly degenerate v_2 bending, and the v_3 asymmetric stretching mode**.** The vibrational energy of a CO_2 vibrational level can be estimated through the anharmonic oscillator approximation [52], described by the following equation [53]:

, (1)

where c is the speed of light, h is the Planck constant, , , , are fitted anharmonic constants (taken from [54] and reported in Table 1), d_k defines the degeneration of the vibrational mode ($d_1 = d_3 = 1$ and $d_2 = 2$) and v_k (with k = 1-3) represent the quantum numbers for v_2 and v_3, respectively.

Table 1. Spectroscopic constants for the calculation of energy levels using (1), obtained from Chedin [54].

Constant	Value (cm^{-1})
ω_1	1335.87915
ω_2	667.20435

ω_3	2361.64697
χ_{11}	-2.99262
χ_{12}	-5.27638
χ_{13}	-19.14044
χ_{ll}	-1.01428
χ_{22}	1.58003
χ_{23}	-12.54184
χ_{33}	-12.50330
γ_{111}	0.02422
γ_{112}	0.00816
γ_{113}	-0.07736
γ_{11l}	0.06316
γ_{122}	-0.05166
γ_{123}	0.09561
γ_{133}	0.06142
γ_{2ll}	0.00702
γ_{222}	-0.00471
γ_{3ll}	0.02587
γ_{223}	-0.02052
γ_{233}	0.01834
γ_{333}	0.00631

Note that expression (1) is modified, compared to [53], to include a number of additional spectroscopic constants (namely) introduced by Chedin [54]. The author calculated also , and g_{22}, which differ somehow from the constants provided by Suzuki [53] and previously used for the calculation of the vibrational energy [29,33]. In the early 90's, Császár [55] and Martin *et al.* [56] found the spectroscopic constants obtained by algebraic contact transformation from Chedin [54] to be the most reliable to compute the quartic force field of CO_2. In addition, they provide a better agreement with the available spectroscopic constants reported by Courtoy [57], and, therefore, we chose them for the calculation of the vibrational energies in this study.

The quantum number l_2 in expression (1) characterizes the angular momentum projection of bending vibrations onto the molecular axis. This number can take the following values:

, (2)

depending if v_2 is odd or even [58]. Finally, with these four quantum numbers, one can specify any CO_2 vibrational level via the notation $CO_2()$, also known as Herzberg's notation.

In the present work, we took into account the so-called accidental Fermi resonance [58–61] among CO_2 vibrational levels with nearly the same vibrational energy. More specific, the interaction between (and leads to a perturbation. These levels, in fact, "repel" each other, meaning that one of them is shifted up and the other down, thus the actual levels are not accurately described by the expression (1). It is important to note that in a symmetric molecule, such as CO_2, the Fermi resonance can happen only between levels with the same quantum number l_2, which arises from the symmetry type of the eigenfunctions describing these vibrational levels [53,58,62]. More on the calculation of the energy correction of perturbed levels can be found in the study of Amat and Pimbert [63] and van den Bekerom *et al*. [64]. In this study, the CO_2 vibrational levels under Fermi resonance are considered as one single effective level, following the same approach as in [9] and [59]. The energy of this effective vibrational level is determined through the average of the energies of all the individual vibrational levels in the effective level, calculated using the anharmonic oscillator approximation (1), while its statistical weight is determined through the sum of the statistical weights of the individual states. These effective levels are denoted in this work by $CO_2()$, where the v_1, v_2 and v_3 quantum numbers correspond to the level with the highest v_1; the ranking number $f$is always equal to $v_1 + 1$ and indicates how many individual levels are accounted for in the effective level. For instance, the level $CO_2(20^00 3)$ stands for the coupling of the three individual levels $CO_2(20^00)$, $CO_2(12^00)$ and $CO_2(04^00)$. The statistical weight g_v of a coupled level $CO_2()$ is determined by the sum of the statistical weights of the various individual levels and only depends on the l_2 quantum number, being 1 for $l_2 = 0$, and 2 (corresponding to two possible directions of rotation) otherwise. For

example, the statistical weight of the $CO_2(20^0 03)$ level is 3, i.e. $g_v = 1 + 1 + 1$. In the purpose of keeping consistency in the notations, the levels that are not coupled by Fermi resonance are still represented by $CO_2()$, using $f = 1$.

As a follow-up of the modelling effort carried out by the N-PRiME (Lisbon) group, this study includes the 72 vibrational levels introduced by [33,34] and extends the description of the symmetric (ν_{12}, i.e. symmetric stretching and bending modes) levels of CO_2, resulting in a total of 101 vibrational levels, which are listed in Table A1 in Appendix A. In particular, the model comprises a full description of the symmetric levels up to 0.5 eV and all the possible combinations with the first five asymmetric levels. Indeed, we do not include all asymmetric mode vibrational levels, as we do not focus on the ladder climbing up to the dissociation limit. In addition, 4 symmetric levels are added to extend the description up to 0.6 eV. Such an extension is intended to fully identify the role of ν_{12} on the excitation of ν_3 and on the heating dynamics, as explained later in the results section.

3. Description of the model

The kinetic model developed for this study is the result of a collaboration between the research groups N-PRiME (IST Lisbon) and PLASMANT (Antwerp). The aim of such collaboration is the establishment of a common procedure to construct a detailed chemistry set for CO_2 low-pressure pulsed direct current (DC) discharges and infer the main pathways characterizing the heating dynamics in this type of discharges. The verification of the model was first tested and carried out using the LoKI (LisbOn Kinetics) simulation tool [65,66]. In this step, we systematically added the vibrational states of CO_2 and the corresponding reactions. Concurrently,

we performed simple tests of the Vibrational Distribution Function (VDF) to verify the correctness of the implementation. The same procedure was then repeated with the ZDPlasKin code [67], validating the procedure. More details on the procedure and a comparison between the two simulation tools will be provided in a future study, with a focus on the verification of numerical models. After the inspection on the vibrational chemistry of CO_2, the model was implemented in the ZDPlasKin code that was used to obtain the results shown here. A description of the 0D kinetic model, solved with ZDPlasKin, is offered in section 3.1. The main steps towards the construction of a detailed chemistry set are (i) the construction of a complete and consistent set of cross sections (c-s) describing the relevant interactions between electrons and heavy gas species (see section 3.2); and (ii) the implementation of scaling laws to calculate the rate coefficients for V-V and V-T exchanges (see section 3.3), for which the experimental values are unknown. Moreover, section 3.4 is dedicated to the inclusion of the relaxation of electronic states in the model. The complete set of reactions solved by the model can be found in Table A2 in Appendix A. The input parameters to the simulations are the discharge pressure, the pulse length, the tube radius and length from experiments [8]. For the simulations presented in section 4.1, the experimental gas temperature profile is used, along with the time-dependent electron density profile estimated from the measured temporal variations of the discharge current and a E/N of 55 Td, as described by [34]. The simulations with self-consistent calculation of the gas temperature are described in section 3.5 and the outcome is presented and discussed in section 4.2. In addition, we tested the model for E/N = 90 Td, as suggested by our calculations presented in section 3.6.

3.1. 0D simulations

The present modelling study has been performed using the ZDPlasKin [67] simulation tool, which provides a self-consistent description of both electron and heavy species kinetics in the plasma. The 0D simulations were run with a pressure fixed at 6.7 mbar and an initial flow rate of 166 sccm of CO_2 at 300 K, in order to reproduce the experimental conditions for the "single-pulse" measurements presented by Klarenaar *et al.* [8]. Both pressure and mass flow rate are kept constant throughout the simulation. Thus, the density of each gas-phase species is multiplied by $p(t = 0)/p(t)$, where p is the pressure in the reactor. Also the velocity q is updated as $q = \dot{m}(t = 0)/\rho(t)$ A, where $\dot{m}$ is the mass flow rate, ρ is the gas density and A is the cross-sectional area of the simulated volume. This is done at every time-step during the simulation. Such modifications are necessary to account for the gas expansion due to increasing temperature and molar flow rate due to dissociation in the plasma. Both effects are incorporated in the variable , the gas expansion factor, which is defined by

(3)

with M being the total number of particles. is initially equal to 1 and decreases when the gas expands and it is included in the calculation of the conversion and product yields. After specifying the initial parameters, the Boltzmann solver BOLSIG+ [68], which is included in the ZDPlasKin tool, is used to calculate the electron energy distribution function (EEDF) using estimated values for E/N and the electron density (n_e) while simulating the active part of the discharge. E/N can be either estimated directly from the experiments or self-consistently calculated from the estimated values of power density (see section 3.6) using Joule's law, with being the conductivity, which is given by . The electron mobility is obtained from the Boltzmann solver, and $e$is the elementary charge. In the afterglow, E/N and n_e are set to zero, because the power deposition is equal to zero and electron impact processes are expected to have a negligible contribution. For the calculation of the EEDF, it is necessary to specify the

scattering cross-sections for electrons colliding with the heavy species in the plasma, along with the initial gas composition and pressure. Once the EEDF is computed, the macroscopic electron properties such as T_e or rate coefficients for the electron-impact reactions are obtained and provided to the chemistry module of the ZDPlasKin tool. At this point, the 0D model solves the temporal evolution of the different species densities according to the following equation,

(4)

in which n_s refers to the density of the species s, index j refers to reaction j and index l refers to the different reactants of reaction j and are the right- and left-hand side stoichiometric coefficients of species s, respectively, taking part in reaction j, k_j is the reaction rate coefficient, and , is the reaction rate, with being the product of densities n_l of species present on the left side of reaction j. BOLSIG+ and the chemistry module are iteratively called to calculate the electron-impact rate coefficients and species densities, respectively, and to update the EEDF and the gas composition in a consistent way. For the chemistry module of the simulation, it is necessary to give as input a chemistry set with the reactions that need to be tested. The systematic addition of the relevant reactions and rate coefficients is detailed in the following sections.

The model described here features the self-consistent calculation of T_3 and T_{12}, which are calculated based on the population of $CO_2(00^0 11)$ and $CO_2(10^0 02)$, respectively. Thanks to the close energies of levels in Fermi resonance with non-Fermi bending levels, and to the similarity of the rate coefficients involving these states, it has been shown that T_{12} is a good descriptor of the excitation of both v_1 and v_2 [8]. In both cases, the vibrational temperature is obtained from

, (5)

where E_1 is the energy of the first v_3 level for T_3 or of the first v_{12} level for T_{12}, with n_1 being the corresponding density, n_0 being the ground-state density of CO_2 and k_B the Boltzmann constant in

J K^{-1}. Moreover, the self-consistent calculation of T_g is also implemented and applied to validate the heating mechanism proposed. More details on this calculation are given in section 3.5.

3.2. Electron kinetics

The first step to develop a kinetic model for a gaseous discharge is the selection of a complete and consistent set of c-s to describe the electron kinetics. The electrons gain energy from the electric field and subsequently redistribute it among different energy channels. Firstly, the EEDF is calculated by solving the steady-state, homogeneous electron Boltzmann equation in the two-term expansion approximation [69]. The electron Boltzmann equation is solved taking into account elastic and inelastic collisions between electrons and CO2($X_1\Sigma^+$) molecules, including vibrational excitation energy losses (corresponding either to the excitation of individual levels or of groups of vibrational levels), superelastic collisions with CO_2 vibrationally excited states, excitation of two groups of electronic states, and ionization. Moreover, complete sets of c-s are incorporated for the dissociation products, namely CO, O and O_2, despite the splitting of CO_2 is very limited under the conditions of study here. The choice of the electron impact c-s set was made upon comparison against the swarm parameters, more specifically the reduced electron mobility and the reduced Townsend effective ionization coefficient. In this context, the electron impact c-s set in [69] provides a very good agreement with the experimental swarm parameters. The inclusion of higher vibrational levels leads to a deviation of the calculated reduced electron mobility in the range of E/N = 20-100 Td, which is relevant to this study and thus poses a threat to the correctness of the simulations. Hence, only the collisional processes contained in the electron impact c-s set of [69] have been used for the numerical solution of the electron Boltzmann equation and the calculation of the EEDF. The set of c-s is available at the IST-

Lisbon database published at LXCat and are described in detail in [69]. Once the EEDF is known, the rate coefficients for each electron-impact excitation process from a state *i* to a state *j* are given by

, (6)

where m_e is the electron mass, *u* is the electron energy, is the electron c-s and *f*(*u*) is the EEDF.

In the context of the electron-impact vibrational excitation (e-V), the transitions from the ground state to the higher vibrationally excited levels that are not included in any of the c-s from the data set [34,69], i.e. and $i = 0$ in v_3, are calculated using the Fridman approximation [26]. The calculation is based on the following semi-empirical formula:

. (7)

This expression allows the scaling of the rate coefficients C_{ij} for any transition between vibrational levels *i* and *j*, provided that the rate coefficient C_{01} is known. The magnitude of the rate coefficient is altered depending on the parameters and , specific of each plasma species. In the case of CO_2, for v_3 and the value of is unknown [26]. Therefore, for the rate coefficients for the stepwise excitation of levels *j* from $i > 0$, we have chosen to set for simplicity (i.e. the magnitude of C_{01} will be equal to C_{12}). The rate constants C_{ji} for superelastic collisions are obtained from the principle of detailed balance [70]

, (8)

where are the threshold energies for the corresponding excitations, and g_i and g_j are the statistical weights of level *i* and *j*. The shift in threshold due to the anharmonicity of the oscillator is taken into account in the detailed balance, where the real energy threshold of the transition is considered.

In order to verify the correctness of the approach, we added systematically the c-s to the data set, along with the calculation of the corresponding e-V rate coefficients, and tested the kinetic

model with a Maxwellian EEDF, ensuring that all the vibrational levels included in the model follow a Boltzmann distribution with T_e. The list of the e-V processes included in this study is available in [34]. This bring us to the inclusion of the V-V and V-T reactions to the model, which is outlined in the next section.

3.3. Vibrational kinetics

A proper investigation of the underlying mechanisms of the heating dynamics in a gas discharge demands a detailed description of the vibrational energy exchanges between molecules. Here, these exchanges are categorized as follows: (i) nearly resonant collisions, with a transfer of vibrational energy from one molecule to another (V-V); (ii) non-resonant collisions, with inter-molecule energy exchange and loss of the energy defect to translational degrees of freedom (V-V-T); (iii) non-resonant collisions, with intra-molecule loss of vibrational energy transferred to translational energy (V-T). The corresponding state-specific rate constants are taken from the survey of Blauer and Nickerson [59]. Nevertheless, this is not sufficient for a full characterization of the vibrational kinetics, since the rate coefficients of the transitions involving higher levels are missing. Several theories have been developed to calculate the state-specific rate constants for vibrational energy exchange in molecular collisions [71]. Approximate, reduced-dimension methods, such as the Schwartz-Slawsky-Herzfeld (SSH) theory for V-T relaxation [72], the Rapp-Englander-Golden theory for V-V relaxation [73] and the Sharma-Brau (SB) theory for V-V relaxation induced by long-range forces [74], are very popular for their simplicity. A more accurate approach can be based on the Forced Harmonic Oscillator (FHO) theory [24,75,76], which is the extension to higher order terms of the same kinetic theory the SSH first order approximation is built on. Recently, *Quasi-classical* Trajectory (QCT)

calculations have also been developed and improved in terms of computational effort, making them a good compromise between calculation time and accuracy [77]. QCT techniques are the only viable approach to full dimensional dynamics and to the calculation of state-to-state collisional cross-sections for systems having more than four atoms, such as CO_2-CO_2 collisions [78]. For instance, Lombardi *et al*. [79] applied QCT and Potential Energy Surface (PES) techniques to the CO_2-CO_2 collision system. The authors found that intermolecular transfers essentially involve rotational and vibrational exchanges, while intramolecular energy transfers efficiently redistribute the energy between symmetric stretching and bending modes, with the asymmetric stretching being fully decoupled if the symmetric levels of the molecule are not sufficiently excited.

In this study, we computed the fundamental transitions given by [59] and scaled the remaining rate coefficients on the basis of the SSH scaling as described in [70] and following an approach similar to Kozák and Bogaerts [29] and Silva *et al.* [9].

Additionally, we found that the list of vibrational energy exchanges of [59] is lacking some important reactions to fully depict the vibrational relaxation processes occurring under the conditions of study. To address this issue, we had to add vibrational exchanges with rate coefficients provided by different literature references and retrieved under different experimental conditions or even computationally calculated. Thus, we believe that this step, along with the selection of the electron impact c-s, represents a major source of uncertainties and, therefore, requires special attention. For instance, we included the nearly resonant collisional up-pumping process along v_3, given by

$$CO_2(00^0 11) + CO_2(00^0 11) \leftrightarrow CO_2(00^0 01) + CO_2(00^0 21), \quad (9)$$

with the rate coefficients computed applying the SB theory by [9]. The rate coefficients for the transitions within higher v_3 levels were obtained with the SB formulation described in [80], which should be valid for low excitation conditions, i.e. low power input, where and T_g remains low. Other CO_2 V-V reactions similar to (9),

$CO_2(00^0 11) + CO_2(01^1 01) \leftrightarrow CO_2(00^0 01) + CO_2(01^1 11)$, (10)
$CO_2(10^0 12) + CO_2(00^0 01) \leftrightarrow CO_2(10^0 02) + CO_2(00^0 11)$, (11)
are also incorporated in the model, with the rate coefficients derived from [81].

The survey of Blauer and Nickerson [59] provides the rate coefficients for only one V-V-T transition, i.e.

$CO_2(00^0 11) + CO_2(00^0 01) \leftrightarrow CO_2(10^0 02) + CO_2(01^1 01) + 495.77$ K, (12)
where $CO_2(10^0 02)$ is the effective level resulting from $CO_2(02^0 0)$ and $CO_2(10^0 0)$, which are strongly coupled by Fermi resonance, as detailed above in section 2. Notwithstanding that, reaction (12) can also result in

$CO_2(00^0 11) + CO_2(00^0 01) \leftrightarrow CO_2(02^2 01) + CO_2(01^1 01) + 495.93$ K, (13)
leading to a transfer of energy from v_3 to pure v_2 levels [82,83]. The branching ratio between (12) and (13) is unknown. However, [82] suggested that the average number of v_2 quanta produced by deactivation of $CO_2(00^0 11)$ is equal to 2.8 in the 190-300 K temperature range. Nevertheless, this value may decrease as the gas temperature increases [84], indicating that the deactivation of v_3 leads to the excitation of both $CO_2(10^0 02)$ and $CO_2(02^2 01)$. With this in mind, we included both (12) and (13), assuming a branching ratio of 50:50. The rate coefficient for (13) was measured to be by Lepoutre *et al*. [82], as reported in [85]. This rate coefficient differs from the one given in [59] for reaction (12). The difference is shown in Figure 1, where the rate coefficients for (12) and (13) are plotted as a function of T_g, in the interval of interest for this modelling study.

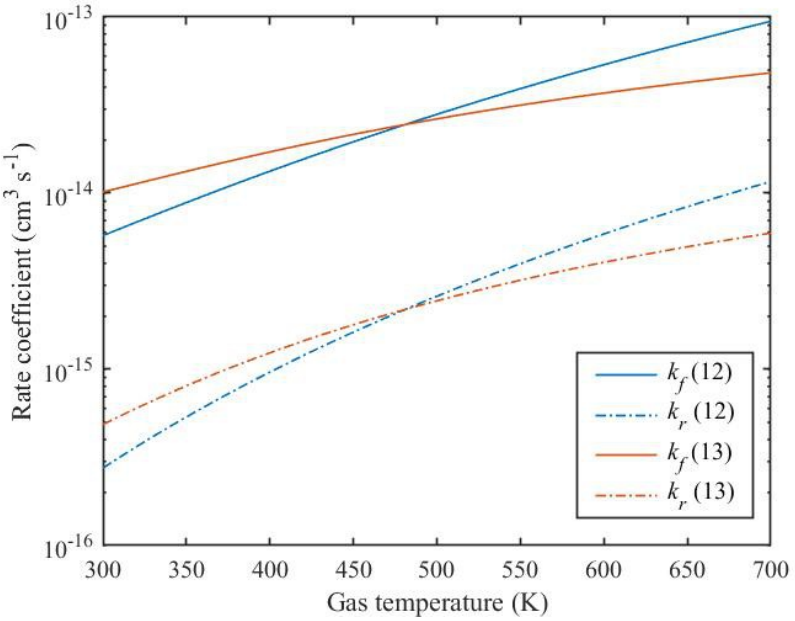

Figure 1. Plot of the forward (k_f) and reverse (k_r) rate coefficients for (12) [59], and for (13), measured by [82], as a function of the gas temperature. The reverse rate coefficients are calculated according to the principle of detailed balance [70].

The comparison displayed in Figure 1 shows that important deviations arise at T_g < 400 K. However, both rate coefficients converge at ca. 480 K, which is right in the middle of the temperature range of study here, although they deviate again at higher temperatures. Moreover, Lepoutre *et al.* [82] measured the deactivation of $CO_2(00^0 11)$ (13) in a low T_g range (190-300 K), which is relevant for the study of radiative transfer processes in the middle atmosphere. Therefore, their rate coefficient may not describe with sufficient accuracy the role of (13) at higher T_g. Following this reasoning, and for consistency with the other vibrational exchanges included in this study, we kept the rate coefficient of (13) equal to the one of (12), and we scaled it for the higher levels using the SSH theory.

At this point, we would like to emphasize that the SSH and SB theories are affected by limitations at high temperatures (T_g > 1200 K) and high vibrational quantum numbers (v_n > 5), which may potentially lead to overestimation of the computed rate coefficients [61]. However, these limitations do not pose a threat to the reliability of the calculations presented here since the experimental measurements [8], used for the validation of the model, were obtained in a low excitation regime, resulting in K.

Starting from the foundations laid by [9], we extended the vibrational description to 101 levels, accounting for a total of ca. 450 V-T, 600 V-V-T and 1700 V-V direct reactions. All the rate coefficients associated with these reactions are fitted from the following expressions dependent on T_g [59]:

, (14)

where *A*, *B*, and *C* are fitting constants.

The inverse reaction rate coefficients are computed from the principle of detailed balance [70]. Further details on the principles and the procedure to construct the vibrational chemistry used in this study can be found in [9].

Another important V-T reaction included in this work is the deactivation of v_3 (15) and v_2 (16) levels by collision with oxygen atoms (V-T O) [86]:

, (15)

with *v*, and

, (16)

with *v* and *w* = *v* - 1. The rate coefficients of reactions (15) and (16) are assumed to be independent of and given by and , respectively [85]. Because of their high rate coefficients, these reactions represent a very efficient quenching mechanism of vibrationally excited CO_2,

which can significantly affect the VDF of v_3 and the heating dynamics, even at relatively low concentrations of O atoms [87] (see section 4.2). The deactivation of higher v_3 and v_2 levels, as well as of mixed levels, is included without any scaling of the corresponding rate coefficients.

The vibrational excitation of the dissociation products of CO_2, i.e. CO and O_2, is not taken into account in this study, since the dissociation degree is very low (< 0.7% with E/N = 90 Td). Its influence on the vibrational excitation of CO_2 will be investigated in a future study, with experimental conditions under which the dissociation degree in the plasma is not negligible.

As we did for the implementation of the e-V transitions, here we added systematically the vibrational exchanges while verifying the correctness of the procedure. In this case, the inspection was done by running a simulation with a very low n_e and T_e as input parameters, thus the VDF is in a Boltzmann distribution with T_g set in the model, if the implementation of new reactions is correct. More details on this verification step will be offered in a future publication.

3.4. Relaxation of electronic states

Along with V-T relaxation, the relaxation of electronically excited molecules can be responsible for the onset of gas heating at the beginning of the discharge pulse. As discussed in the Introduction, little attention has been paid to the mechanism of FGH in CO_2 non-equilibrium discharges. We believe that FGH has been disregarded by the modelling investigations of such discharges due to assumptions made on E/N and the description of electronic states, which is still very challenging in the case of CO_2. However, in this study, we aim to demonstrate that the role of electronic states is not limited to the promotion of CO_2 dissociation, under the typical conditions of operation in low-pressure pulsed glow discharges (i.e. E/N = 50-90 Td, T_e = 2-3

eV). The contribution of the relaxation of $O(^1D)$ and $CO(a^3\Pi)$ excited states was recently studied by [46] in a nanosecond pulsed discharge with high specific deposited energy (eV/molecule). This led to the estimation of E/N 150-250 Td, thereby a significant part of the discharge energy goes to electronic excitation. The authors well described the FGH phenomenon with a 1D axisymmetric model, validating their kinetic scheme with experimental results. In their model, the rate of direct electron-impact dissociation of CO_2, to give $O(^1D)$ and $CO(a^3\Pi)$ as products, along with the corresponding ground states $O(^3P)$ and $CO(^{1+})$, is calculated from (6) by using Phelps c-s for electronic excitation, with threshold energy of 7 and 10.5 eV [88] for

(17)

and

, (18)

respectively. This choice was motivated by the observations of Babaeva and Naidis [89], who compared estimates of the CO_2 conversion efficiency, obtained using Phelps [88] or Polak [90] c-s for dissociation, with available experimental data. As an outcome, the authors [89] suggested the use of one of the two Phelps c-s, either with 7 or 10.5 eV threshold energy, as they provided a better agreement with the measured conversion efficiencies than Polak c-s, which underestimate the efficiency. A plot of the c-s from [88] and [90] as a function of the electron energy is provided in Figure 2. However, the sum of both Phelps c-s leads to overestimation of the conversion [89] and yet it is necessary to accurately compute the EEDF [69]. Moreover, the use of Phelps c-s for CO_2 dissociation is only recommended for E/N 90 Td, larger than the focus of this study. On the other hand, previous contributions [91,92] underlined the importance of Polak c-s via numerical modelling and experiments for E/N < 100 Td. These c-s describe dissociation reactions (17) and (18), with energy threshold of ca. 7.5 and 11.9 eV, respectively.

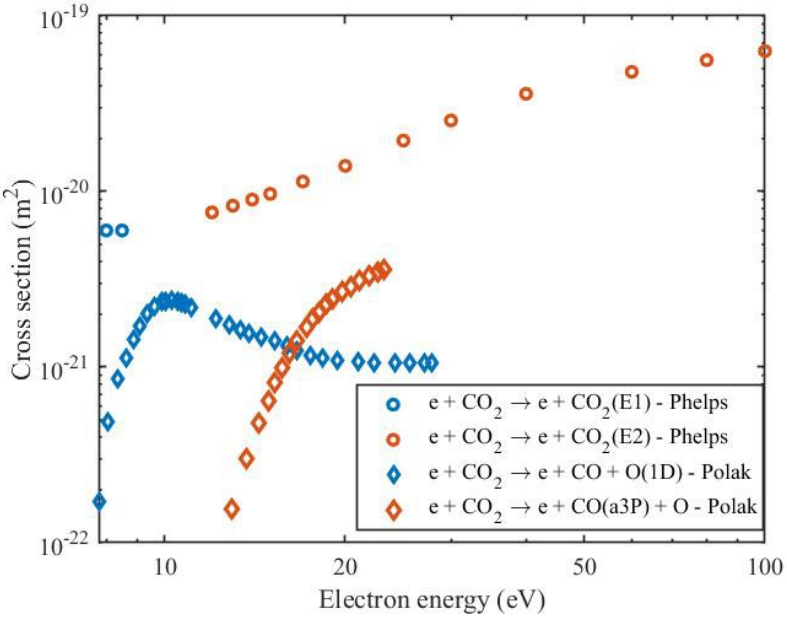

Figure 2. Phelps [88] and Polak [90] cross sections for electronic excitation and dissociation, respectively, as a function of the electron energy. CO_2(E1) and CO_2(E2) represent a group of electronic states with a threshold energy of 7 and 10.5 eV, respectively [88].

The comparison between the magnitude of Phelps and Polak c-s, depicted in Figure 2, indicates that the former set likely includes pure electronic excitation channels beyond electron-impact dissociation. This further encouraged us to use Polak c-s for the calculation of the CO_2 dissociation rate. However, as anticipated earlier, Phelps c-s are needed to compute the EEDF as they assure a valid prediction of the swarm parameters when used in a two-term Boltzmann solver and for E/N < 1000 Td [69]. In particular, the replacement of the Phelps with the Polak set leads to miscalculation of the reduced Townsend effective ionization coefficient, highlighting that some electron energy losses, which are not ascribable to dissociation, are missing in [90]. Therefore, considering the above observations, we kept the Phelps c-s for the excitation to CO_2(E1) and CO_2(E2), which are already integral part of the LXCat set [69] used in this work,

solely for the calculation of the EEDF and, thus, of the E/N, as recommended in [69] and used in [93]. However, we used the Polak set for the calculation of the rate of electron-impact CO_2 dissociation and a new set, derived from the subtraction of the Polak to the Phelps c-s, for the rate of excitation of CO_2 to CO_2(E1) and CO_2(E2). This has been done with the assumption that the fraction of electron energy that is not spent into dissociation goes into electronic excitation [91,92] and, subsequently into heat. The approximation on the calculation of the rate coefficients for electronic excitation of CO_2 is needed in order to reduce any possible overestimation on the total production of electronic states due to the sum of Polak's c-s (for dissociative states only) and Phelps' c-s (where dissociative states are likely to be already included). We believe that the model could be further optimized with a deeper knowledge on the nature of the electronic states of CO_2 and by having a complete set of c-s for CO_2 which allows to discriminate between dissociative, radiative and non-radiative (whose collisional quenching releases heat) electronic states.

The electronic states included in this modelling work are listed in Table 2.

Table 2. Electronic states included in the model and their energy thresholds.

Electronic state	Energy threshold (eV)
CO_2(E1)	7
CO_2(E2)	10.5
CO($a^3\Pi$)	6
O(^{1}D)	1.96

The inclusion of O(^{1}D) and CO($a^3\Pi$) is motivated by their formation as consequence of reactions (17) and (18). The relaxation rate coefficients for these species can be found in Table A2 in Appendix A, and more information is available in [93]. The exact composition of the lumped CO_2(E1) and CO_2(E2) excited states is unknown, and there is a lack of kinetic data for the

relaxation of electronically excited CO_2 molecules in literature. Therefore, we adopted a relaxation rate coefficient equal to the sum of and , assuming that CO_2 excited states behave similarly to . Deeper investigation and characterization of the electronic excitation and relaxation of CO_2 are urgently needed to reduce the number of approximations required for modelling the heating dynamics.

3.5. Self-consistent calculation of

The results presented in section 4.2 were obtained with simulations featuring the self-consistent calculation of . To this end, the model solves the following heat balance equation

(19)

where N is the total heavy-particle density, is the ratio of specific heats, is the gas heating power density due to elastic electron-neutral collisions, is the heat released (or consumed) in reaction j, and is the power density loss due to exchanges with the surroundings. For CO_2, is taken from Silva *et al.* [45], who estimated it based on [94], and .

Considering a gas discharge under isobaric conditions and assuming that the heat conduction is the dominant cooling mechanism, we considered the external cooling term as follows

, (20)

in which is the gas thermal conductivity, and is the wall temperature taken as 300 K. In this work, the gas thermal conductivity is W m^{-1} K^{-1} as previously used by [17,32,45] and estimated from [95] for CO_2. The radius of the reactor r is set to 1 cm [8].

The contribution of reaction j to the gas heating (, in K s^{-1}) is recorded throughout the simulation according to the following expression, derived from the heat balance equation

. (21)

Analogously, the electron energy loss rate (, in eV s^{-1}) is computed as follows:

, (22)

where is the rate and the energy threshold of the electron-impact reaction *j*. and will be later used to describe the contribution of different classes of reactions to the electron energy deposition onto distinct processes, and to the gas heating, respectively.

3.6. Estimation of the reduced electric field (E/N)

The E/N is an essential parameter to define the energy transfers between electrons and heavy species in discharges where the dynamics is dominated by electron impact processes, whose rate coefficients depend on E/N. The balance between electron creation by ionization and loss by electron attachment, volume recombination and diffusion to the walls determines the sustaining E/N. In particular, under the conditions studied here, dissociative electron attachment () constitutes the main electron loss channel, producing stable negative ions , as well as , which are formed by [96]. The inverse reactions, i.e. electron detachment (see Table A2 in Appendix A), are slower than attachment, determining a reduction in n_e, which needs to be replenished by additional ionization in order to sustain the discharge. Therefore, the E/N will be mainly defined by the balance between electron attachment and volume recombination and ionization.

Klarenaar *et al.* [8] estimated a E/N of 60 Td by measuring the potential difference over two metal rods pointing inside the positive column of the reactor, while maintaining a continuous discharge of 50 mA at 6.7 mbar. From this value, they calculated n_e as 10^{10} cm^{-3}, using the electron drift velocity estimated from [97]. Later, Grofulović *et al.* [34] calculated a E/N of 55 Td for the same conditions, in good agreement with [8]. In order to further confirm these

calculations, we performed a self-consistent calculation of E/N and n_e using the current profile provided by [8] and a fixed voltage of 1.5 kV. The E/N is computed as follows:

, (23)

where is the power, calculated as the current multiplied by the voltage, V_R is the reactor volume and e is the elementary charge.

The electron density n_e is computed by ZDPlasKin and its magnitude is a result of a balance between electron-impact processes (i.e. ionization and attachment) and volume recombination reactions. The self-consistently calculated E/N, along with the corresponding T_e, and n_e are plotted in panels (a) and (b) of Figure 3, respectively, as a function of the discharge time.

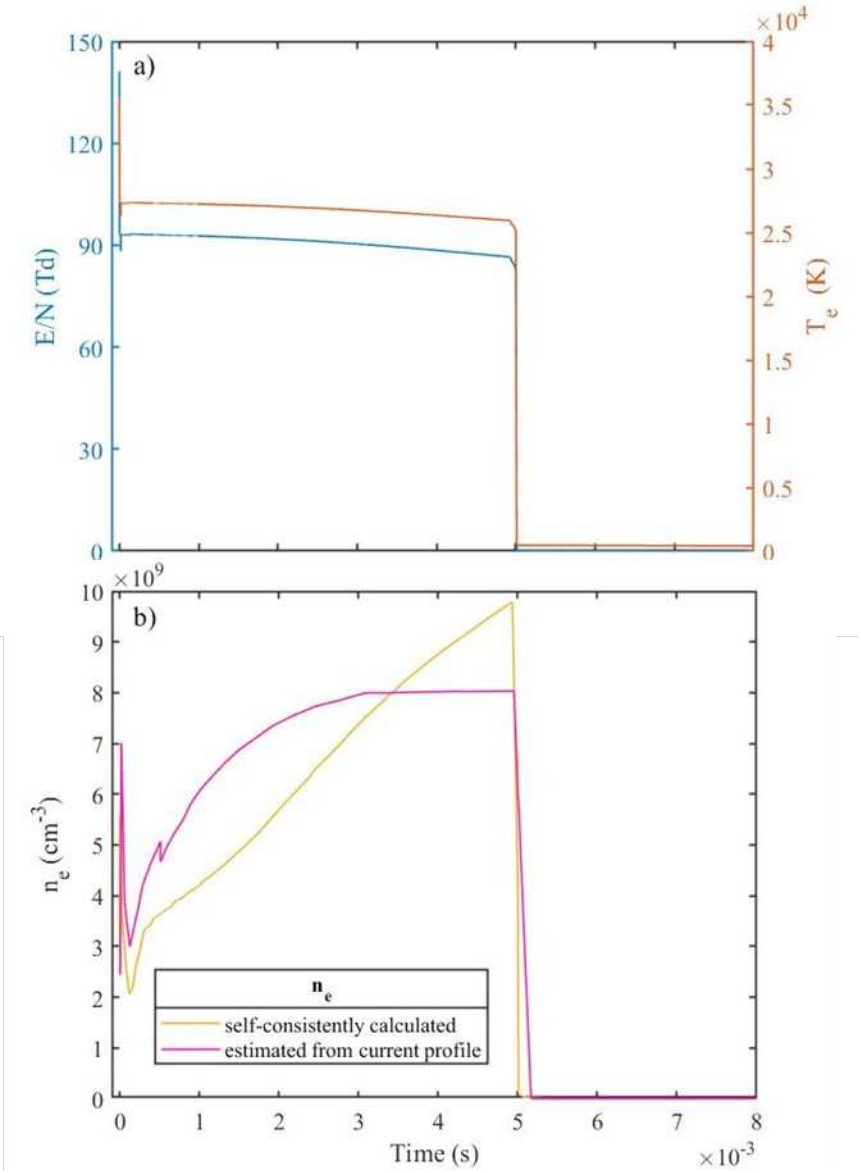

Figure 3. Time-evolution of (a) self-consistently calculated E/N and T_e and (b) n_e, self-consistently calculated and estimated from the experimental current profile [8,34].

Our simulations suggest a larger E/N than the previous estimations (i.e. ca. 90 Td vs 60 Td [8] and 55 Td [34]), with a corresponding T_e of ca. 27000 K (Figure 3(a)). The difference with E/N estimated from the experiments [8] can be ascribed to the fact that the measurements of the potential difference were performed in a continuous discharge and not in a pulsed regime. In the latter situation, ionizing conditions are needed to build up the electron density to sustain the

discharge, at least at the beginning of the pulse. In other words, E/N is likely to be larger than 60 Td for a good part of the pulse. Instead, the differences in the calculated values of the self-consistent sustaining field between [34] and the present calculations are associated with the different discharge models used and still require further investigation. For instance, [34] only considered CO_2^+, whereas, in our chemistry set, additional positive and negative ions are also included. As pointed out at the beginning of this paragraph, the negative ions O^- and CO_3^- are important products of the dissociative electron attachment reactions, which reduce n_e and, consequently, increase E/N. In view of this, a detailed comparison of the different model formulations will be carried out in a future publication.

It is worth mentioning that the total length of the reactor tube, i.e. 23 cm, was used to calculate V_R and, therefore, the power density (P/V_R). This means that the power density may be larger than in our calculations if the plasma does not fill completely the entire volume, which in turns leads to higher E/N according to equation (23). On the other hand, the voltage evolution during the pulse is not known [8] and the assumption of a fixed value may be not accurate. Indeed, Damen *et al*. [99] displayed the voltage profiles for similar conditions in the same glow discharge reactor of [8]. The authors showed that the voltage magnitude is not constant during the active phase of the discharge, dropping significantly during the first millisecond to maintain the current constant at 50 mA. The unsteadiness of the voltage directly affects the computation of the power density and leads unavoidably to inaccurate n_e, as shown in Figure 3(b), and to the E/N and T_e evolutions, displayed in Figure 3(a). Therefore, in our simulations, we kept the n_e profile estimated from the experimental current profile and we tested two values of E/N, i.e. 55 Td, for comparison with [34], and 90 Td, as an average value of the profile shown in Figure 3(a). Additional simulations that we performed with a range of E/N values also support the choice of

90 Td. More specifically, a E/N of 94 Td is needed to sustain the discharge and compensate for the electron losses to dissociative attachment during the onset of the discharge. After that, E/N should slowly decrease; otherwise, n_e exceeds the estimation based on the current profile. Hence, we believe that 55 and 90 Td represent two extreme situations that can describe the end and the beginning of the discharge pulse, respectively. In the next sections, we present the simulation outcomes for both E/N values, first without and then with self-consistent calculation of T_g. The effect of E/N on the gas heating dynamics is discussed in section 4.2.

4. Results and discussion

4.1. Validation of the vibrational kinetics

The investigation of the vibrational kinetics by means of a kinetic model must first be based on a confirmation of the kinetic scheme with experiments. To this end, the "single-pulse" measurement performed by Klarenaar *et al.* [8] in a pure CO_2 glow discharge represents an ideal benchmark for the validation of a 0D kinetic model. Indeed, this measurement was already used for this purpose by Grofulović *et al.* [34]. The authors demonstrated that their model was able to predict in good approximation the evolution of T_3 while introducing the experimental T_g evolution, the n_e profile estimation and a E/N of 55 Td as input parameters. The very good agreement between the model predictions and the experimental results verified the description of the kinetics of v_3. As a follow-up to their work, we started our modelling study from the simulations performed by [34] and we replicated the comparison with the experimental temperature profiles to validate the changes we have implemented since then. The comparison is illustrated in Figure 4.

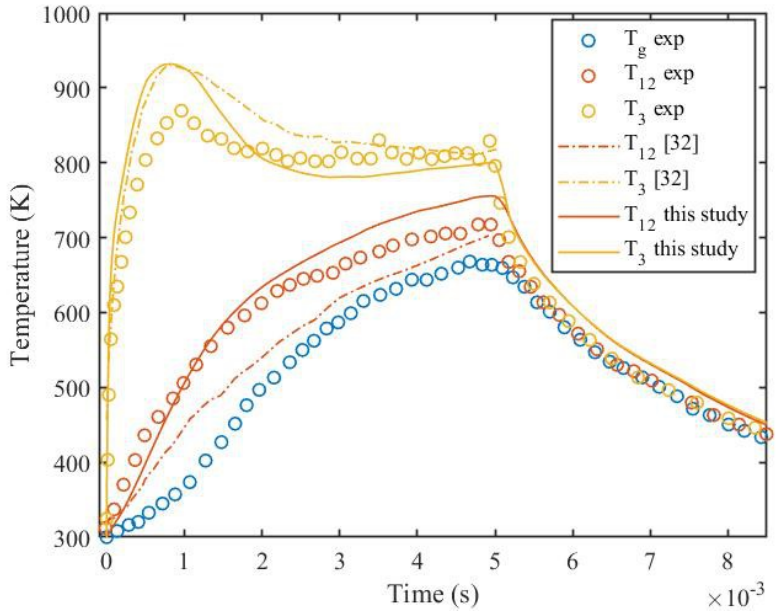

Figure 4. Time-evolution of T_{12} and T_3, measured and digitalized from [8] (circles), simulated and digitalized from [34] (dash-dotted lines), and simulated in this study (solid lines). The experimental T_g profile, used for the simulations, is also plotted.

The new chemistry set refines the agreement with the experimental vibrational temperature profiles when compared to the previous effort [34]. In particular, T_3 and T_{12} show similar evolutions during the first millisecond in the pulse, until the peak in T_3 is reached. After that, a deviation in the model predictions arises: our T_{12} more or less follows the experimental trend whereas T_{12} calculated in [34] relaxes to T_g. Our reaction analysis indicates that the $CO_2(10^00^02)$ level, from which T_{12} is derived, is mostly populated by e-V, V-V and V-V-T reactions at 1 ms. and T_g is still too low to have an important contribution from V-T reactions. To explain the discrepancy of the results, note that in [34] while considering the complete vibrational kinetics of [59], the repeated reaction $CO_2(11^102) + CO_2(01^101) \rightarrow CO_2(10^002) + CO_2(10^002)$ was badly

adjusted to $CO_2(11^102) + CO2(00^001) \rightarrow CO_2(10^002) + CO_2(10^002)$. The latter reaction, not considered in this study, leads to an underestimation of the higher bending and symmetric levels ($v_2 > 2$ and $v_1 > 1$) at short-time scales ($t < 5$ ms) of the plasma pulse. Notwithstanding this correction, the temperature of the symmetric levels was still underestimated compared to the experiments. Therefore, the reason for the different T_{12} is to be sought elsewhere. Specifically, $CO_2(00^011) + CO_2(00^001) \leftrightarrow CO_2(02^201) + CO_2(01^101)$ was only introduced in this study; analogously to reaction (12), this V-V-T reaction populates v_{12} at the expense of v_3. The close coupling via efficient V-V exchanges of $CO_2(02^201)$ and $CO_2(10^002)$ causes an increase in T_{12}, explaining the improved agreement with the experiments. These results confirm the importance of the additional V-V-T process to describe the vibrational kinetics of both v_3 and v_{12}, whose evolutions are closely related. Moreover, Grofulović *et al.* [34] found that the populations of some v_{12} states were underestimated by their model compared to the experiments. The temporal evolution of the calculated and measured normalized populations of $CO_2(v_10^00f)$, $CO_2(0v_2^{v2}01)$, and, in addition, $CO_2(00^0v_31)$ are presented in panels (a), (b) and (c) of Figure 5, respectively.

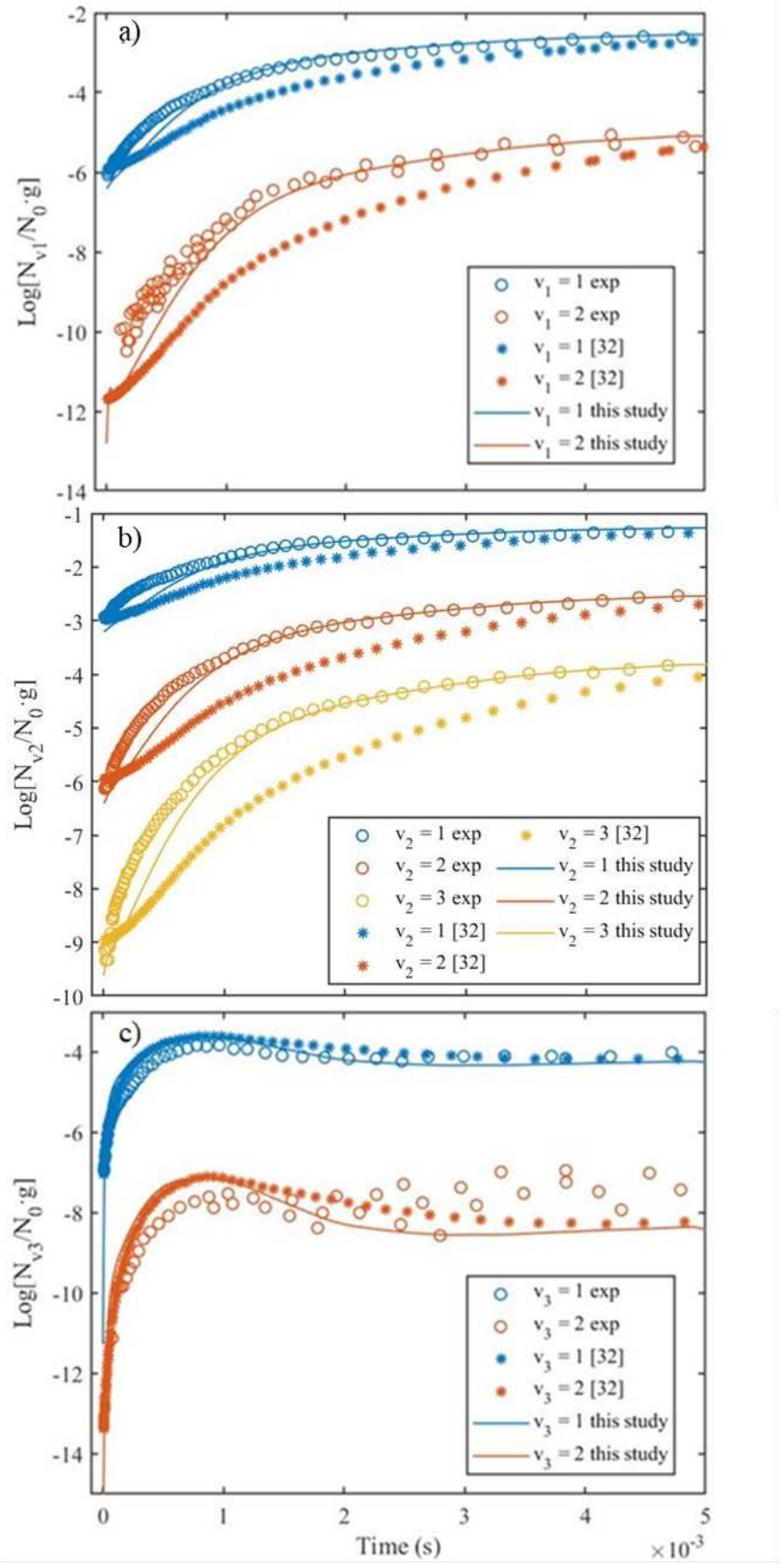
a)
Log[N_v1/N_0·g]
v_1 = 1 exp
v_1 = 2 exp
v_1 = 1 [32]
v_1 = 2 [32]
v_1 = 1 this study
v_1 = 2 this study
b)
Log[N_v2/N_0·g]
v_2 = 1 exp
v_2 = 2 exp
v_2 = 3 exp
v_2 = 1 [32]
v_2 = 2 [32]
v_2 = 3 [32]
v_2 = 1 this study
v_2 = 2 this study
v_2 = 3 this study
c)
Log[N_v3/N_0·g]
v_3 = 1 exp
v_3 = 2 exp
v_3 = 1 [32]
v_3 = 2 [32]
v_3 = 1 this study
v_3 = 2 this study
Time (s)
×10^-3

Figure 5. Normalized density of several states (a) in the symmetric stretching mode, (b) in the bending mode and (c) in the asymmetric stretching mode of vibration as a function of the discharge time. The circles corresponds to the experimental data [8] (digitalized from [34]), the asterisks to the calculations of [34] (digitalized) and the solid lines to our calculations.

For v_{12}, our model results are in very good agreement with the experimental data (Figure 5(a,b)), displaying a growth of the vibrational populations closer to the experiments than the predictions of [34]. In fact, the additional V-V-T transfer considered in this study speeds up the redistribution of the energy from v_3 to v_{12}. Figure 6 shows that the characteristic relaxation rate coefficient of V-V-T transfers is right in between typical V-V and V-T transfer rate coefficients.

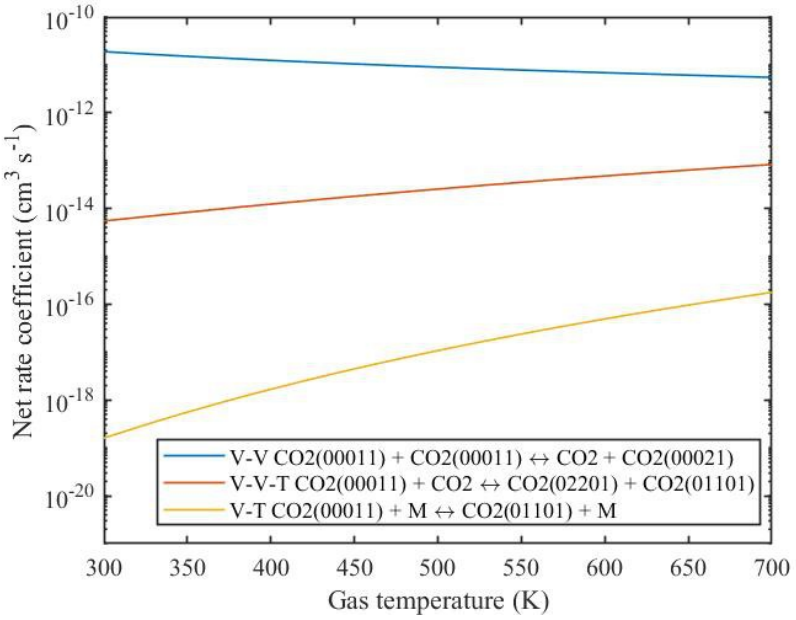

Figure 6. Net (forward minus reverse) rate coefficients of the main relaxation reactions of the first asymmetric level of CO_2 as a function of the gas temperature.

Despite V-V is a faster transfer, V-V-T and V-T reactions represent a nearly irreversible loss of energy for v_3 to v_{12}, since V-T from v_{12} is a very efficient channel of loss of vibrational quanta and, consequently, heating, as demonstrated in the next section and pointed out in [100]. Therefore, V-V-T relaxation can be identified as a relevant mechanism determining the timeframe for a significant T_3-T_g non-equilibrium.

Nevertheless, some underestimation of the growth of the v_{12} populations, along with a slight overestimation of the v_3 population, is still present during the onset of the discharge (cf. Figure 5). This discrepancy indicates that fast energy transfer mechanisms from v_3 to v_{12} may still lack in our model. As suggested by [34], collisions with O_2 molecules or excited atoms may play a role here, even though the CO_2 dissociation degree is typically very low at the beginning of the pulse. Alternatively, V-V-T relaxation may be faster than dictated by the rate coefficient proposed by Blauer [59] at the beginning of the pulse, at 300 K, as highlighted by the comparison with Lepoutre [82] in Figure 1 above.

As explained in section 3.6, our self-consistent calculation of E/N suggested that at least 94 Td is needed to sustain the discharge during the onset phase and that E/N > 55 Td is likely to persist throughout the pulse duration. This considered, we tested a E/N of 90 Td, as averaged from Figure 3(a), to investigate the effect into vibrational excitation. The comparison between the vibrational temperature evolutions for a fixed E/N of 55 and 90 Td is shown in panel (a) of Figure 7, while in panel (b), the electron energy deposition rate into different excitation processes as a function of time is depicted for the same conditions.

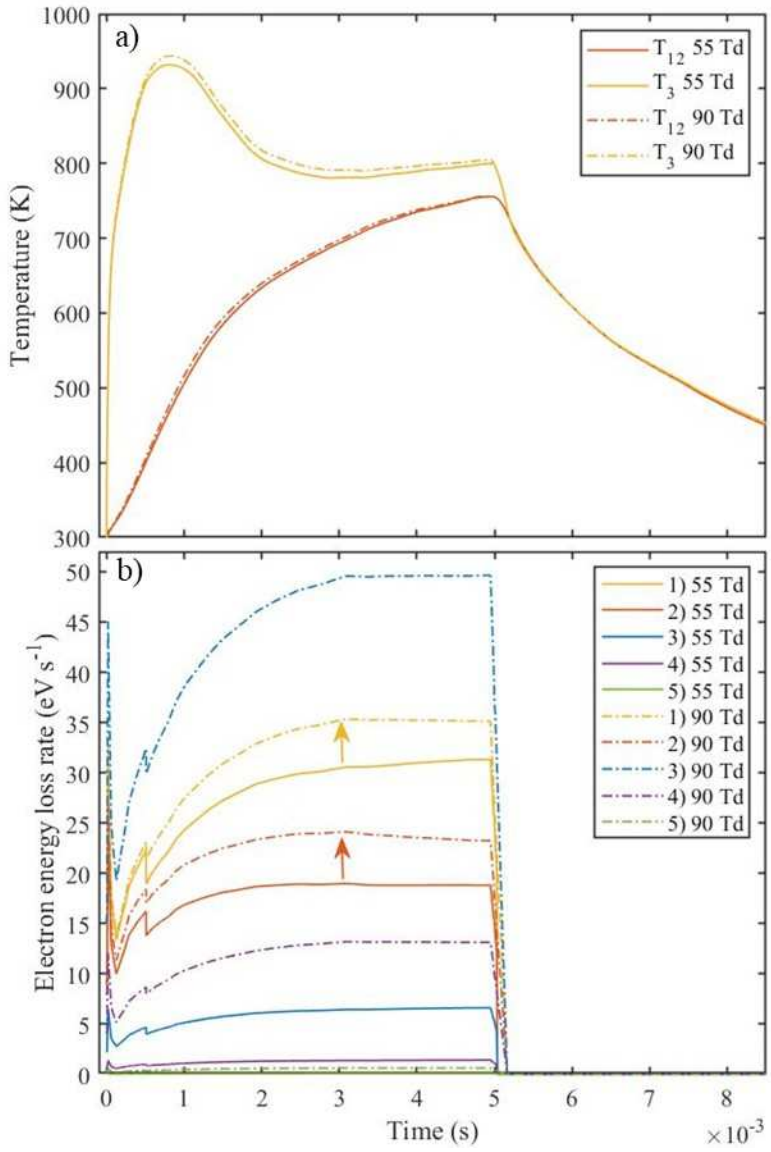

Figure 7. (a) Simulated time-evolution of T_{12} and T_3 for a fixed E/N of 55 Td (solid lines) and 90 Td (dash-dotted lines); (b) electron energy loss rate to (1) asymmetric stretching, (2) symmetric levels, (3) electronic excitation, (4) direct dissociation and (5) other processes (namely ionization, attachment and elastic scattering).

The choice of the E/N significantly affects the way the energy is transferred from the electrons to the different degrees of freedom and excitation channels. Indeed, at 90 Td, clearly more electron energy (ca. 5 eV s^{-1} more) is transferred to the asymmetric stretching and symmetric vibrational levels, as well as to the electronically excited levels (increase of up to 45 eV s^{-1}), and to direct dissociation (ca. 10 eV s^{-1} more). However, the increase in energy deposited into vibrational levels, highlighted by the arrows in panel (b) of Figure 7, does not determine a substantial increment in vibrational temperature, in panel (a). Indeed, the extra energy deposited is promptly distributed over the entire array of levels through V-V-T and V-T relaxation, whose efficiency increases with T_g. Hence, we consider the vibrational kinetics description proposed in this study validated for the interval of E/N relevant for the pulsed glow discharge experiments. Notwithstanding this, a E/N of 90 Td means a larger amount of energy relocated from the electrons to the heavy species compared to 55 Td, triggering different excitation and heating channels. In this connection, a deeper discussion is given in the next section.

4.2. Gas heating dynamics

While the validation of the vibrational kinetics can be conducted by imposing a T_g profile as input parameter for the model, as demonstrated in previous section, the same cannot apply for the study of the gas heating dynamics. In fact, panel (b) of Figure 7 shows that the selection of the E/N determines the excitation routes that are activated, among which vibrational excitation is only one of the possible pathways, and to which extent they are energized. To verify the impact of E/N on the gas heating dynamics, we performed simulations with self-consistent calculation of T_g. The outcome for E/N = 55 and 90 Td, compared against the experiments, is reported in Figure 8.

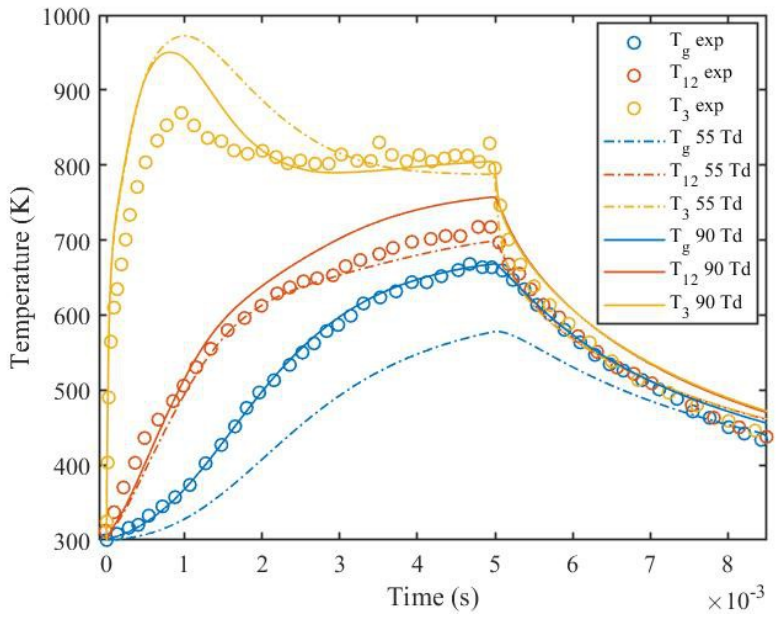

Figure 8. Experimental (circles) and simulated (dash-dotted lines E/N = 55 Td; solid lines E/N = 90 Td) temperature profiles as a function of the discharge time.

Interestingly, the choice of the E/N within the range of interest for this study does affect the vibrational excitation of CO_2. In accordance to Figure 7(b), the T_g profile in Figure 8 is now dependent on the chemistry that is activated by the electrons. Therefore, an overall lower excitation regime determines a diminished heating rate. In general, E/N = 90 Td provides a better

agreement with the experiments, confirming our hypothesis that E/N > 55 Td endures throughout the pulse length.

With attention paid to the afterglow in Figure 8 i.e. t > 5 ms, it is visible that both simulated T_{12} and T_3 lie slightly above the experimental values for long time, without fully relaxing to T_g. The experimental profiles instead indicate that thermalization between vibrational and translational degrees of freedom is reached in 1 ms after the pulse on-time. A comparison with [45] for the same experimental conditions suggests that wall deactivation of vibrationally-excited CO_2 molecules, which is not included in our study, may help in further refining the agreement with the experiments in the post-plasma region. Nevertheless, under the conditions tested, we expect the contribution of this deactivation mechanism into the gas heating to be very small compared to V-T relaxation.

Thus, in order to investigate the relevant heating sources at 55 and 90 Td, and to picture the heating dynamics, we plotted in Figure 9 the contributions of the most relevant reactions, expressed as heating rates, as a function of the discharge time.

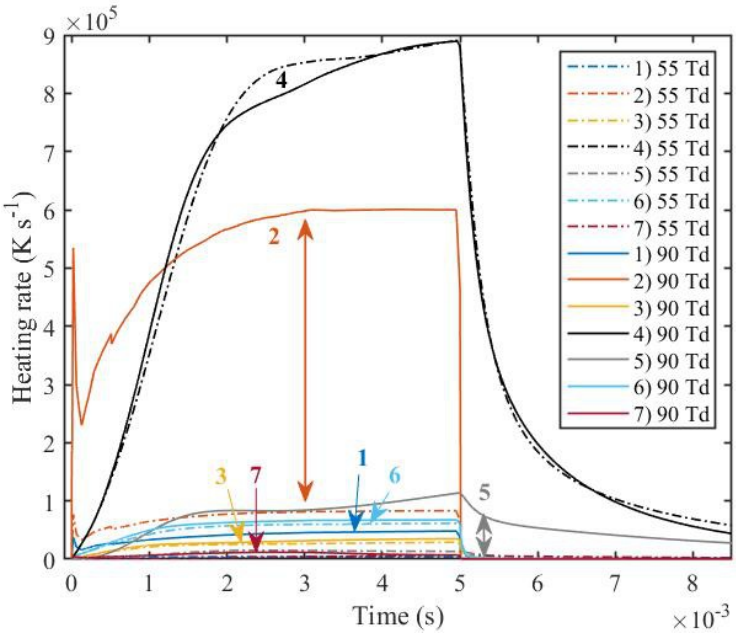

Figure 9. Calculated evolution of the heating rate from: (1) relaxation of CO($a^3\Pi$) and O(^{1}D); (2) relaxation of CO_2(E1) and CO_2(E2) electronic states; (3) V-T relaxation from v_3 to v_{12}; (4) V-T relaxation of v_{12}; (5) V-T deactivation by collisions with O atoms; (6) V-V-T relaxation; (7) other reactions (namely electron-ion recombination, ion-neutral, V-V relaxation, thermal reactions and electron-neutral elastic scattering).

This comparison indicates that V-T and V-V-T relaxation contributions are barely changed between 55 and 90 Td, suggesting that the underestimation of the gas heating, at 55 Td, comes from elsewhere. Indeed, the double arrows in Figure 9 evidence the most relevant differences between the two cases. Of particular interest is the striking increase in vibration-translation deactivation by O atoms and in electronic relaxation. While the former becomes important towards the end of the pulse, the latter strictly follows the current profile and is a result of a larger fraction of energy deposited into CO_2(E1) and CO_2(E2) by electrons at 90 Td (Figure 7(b)). In fact, turning off this process would reflect into overpopulation of v_3, resulting in a T_3 peak value of nearly 1000 K. During the same timeframe (i.e. 1 ms), T_g would be underestimated

to a bigger extent than setting E/N = 55 Td, confirming the necessity of including this relaxation process into the description of the heating dynamics. In particular, the relaxation of CO_2 electronic states is a source of FGH (i.e. with characteristic relaxation times smaller than V-T and V-V-T processes [44]) which smooths out the T_3 peak and reduces the duration of the T_3-T_g non-equilibrium. Note that its fast kinetics is highlighted by the spike at the very beginning of the pulse (see solid curve (2) in Figure 9). Indeed, the production of electronic states strongly depends on n_e and the consequent quenching happens at the sub-microsecond scale, depending on the pressure. Thus, excitation and de-excitation are nearly simultaneous and, therefore, the corresponding heating mechanism accurately resembles the current profile. On the other hand, the vibrational excitation is faster than the relaxation at low temperatures, which is the basis for vibration-translation non-equilibrium. Hence, the V-T profile (curves (4) in Figure 9) is shifted in time, eventually crossing over into the afterglow, where the electron kinetics is fully quenched. The existence of FGH in pure CO_2 was already brought to light by [46], although their study covered a range of E/N 150-250 Td. On the other hand, van de Steeg *et al*. [14] demonstrated that in pure CO_2 pulsed MW plasma, for a similar interval of E/N, V-T relaxation is responsible for up to 50% of the total heating rate, suggesting that the remaining part most likely comes from electronic relaxation. Their observations are in good agreement with our calculations. Specifically, Figure 10 shows that after ca. 1.5 ms, the contribution of CO_2(E1) and CO_2(E2) collisional quenching stabilizes around 35% of the global heating rate, while V-T from v_{12} contributes for ca. 50%. During the first millisecond in the pulse, however, electronic relaxation is the leading heating pathway, whereas the afterglow is dominated by V-T relaxation from v_{12} and V-T deactivation upon collision with O atoms. In fact, in the afterglow the

electronically excited states are quickly quenched and the thermal balance is ruled by V-V, V-T and thermal conductivity, in agreement with [45].

Figure 10. Percentage contribution to the gas heating rate from: (1) relaxation of CO($a^3\Pi$) and O(^{1}D); (2) relaxation of CO_2(E1) and CO_2(E2) electronic states; (3) V-T relaxation from ν_3 to ν_{12}; (4) V-T relaxation of ν_{12}; (5) V-T deactivation by collisions with O atoms; (6) V-V-T relaxation; (7) other reactions (namely electron-ion recombination, ion-neutral, V-V relaxation and thermal reactions and electron-neutral elastic scattering). Note that the contributions are stacked in order from (1) to (7).

This last finding highlights the relevance of O atom kinetics to describe the vibrational kinetics of CO_2, as pointed out by [87]. Indeed, at the end of the pulse, the CO_2 conversion is only 0.7%,

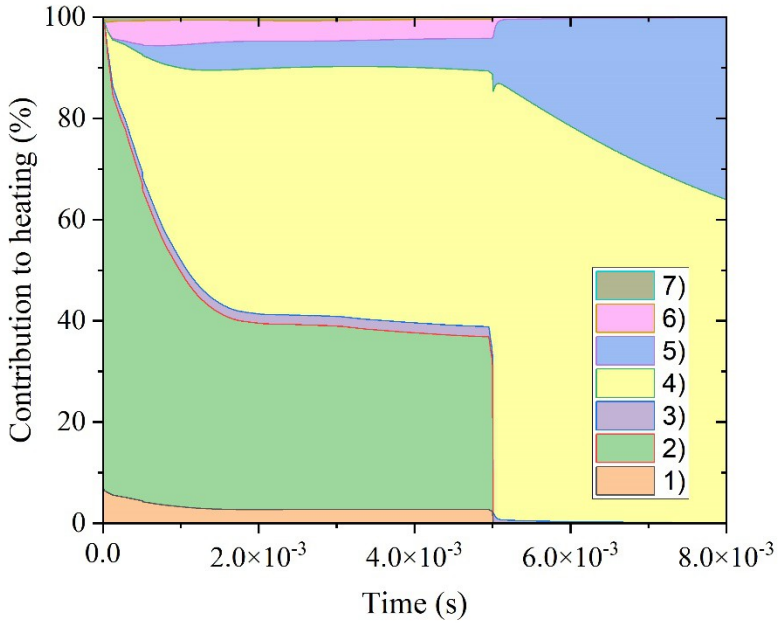

corresponding to an O atom fraction of 0.6% and, yet, it is responsible for ca. 5% of the heating during the pulse and up to 35% in the afterglow. However, we would like to stress that the

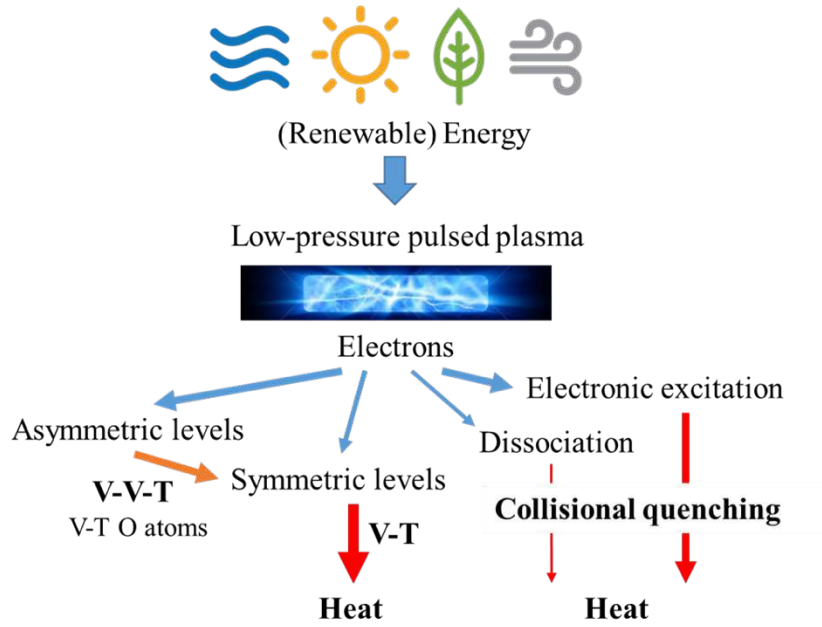

effects of the dissociation products on vibrational excitation and gas heating will be more accurately addressed in a future study, and this observation further motivates us to prosecute it.

With the information collected in this modelling work, we are now able to propose a gas-heating scheme for a pure CO_2 pulsed low-pressure plasma, which is depicted in Figure 11.

Figure 11. Schematic overview of the flow of energy in a pure CO_2 low-pressure pulsed plasma. The red arrows stand for the main heating mechanisms involved: vibration-vibration-translation (V-V-T) relaxation, vibration-translation (V-T) relaxation and V-T deactivation by collisions with oxygen atoms (V-T O atoms) and collisional quenching of electronic states coming from direct excitation or electron-impact dissociation of CO_2.

In a typical implementation of plasma technology for CO_2 recycling, the energy from renewable sources is supplied as electricity to the system. Thus, the plasma source is turned on and a

plasma is ignited in the gas. The electrons collide with CO_2 molecules and a fraction of their energy is transferred into dissociation. The excited dissociation products, $CO(a^3\Pi)$ and $O(^1D)$, contribute to the gas heating through collisional quenching with heavy species. Besides that, an important fraction of the electron energy is spent into excitation of electronic states of CO_2, which promptly relaxes to heat. The rest of the electron energy goes into vibrational excitation; of this, more than half is deposited into v_3 and the rest into v_{12}. The energy stored in v_3 is then distributed over v_{12} by V-V-T relaxation and partially by V-T deactivation upon collision with O atoms (V-T O). Finally, the energy is transferred efficiently to translational degrees of freedom due to fast relaxation of low-lying v_{12}, accounting for a large part of the total heat.

The presence of these multiple channels for gas heating reduces the extent and the timeframe to exploit V-T non-equilibrium in CO_2 plasmas. E/N < 90 Td would be required to limit the dispersion of electron energy into electronic excitation and, consequently, heat. On the other hand, high E/N are necessary to ionize the gas and sustain the discharge in CO_2, due to n_e depletion through efficient electron attachment. This means that, at the beginning of the discharge pulse, electron energy is unavoidably lost to other excitation processes than vibrational excitation. Therefore, the redefinition of the conditions suitable for a consistent and exploitable vibrational excitation, as well as its possible role into dissociation, is highly desirable. In this regard, we aim to provide more insights in a future study, where we will focus on the dissociation of CO_2 and its effects on the heating dynamics.

5. Conclusions

Plasma technology is very promising to convert CO_2 and store excess of energy from renewable sources into valuable compounds. Experimentally, evidences for very energy-efficient conversion (up to 90%) were provided in the past. The key of these successful experimental results may lie behind vibrational excitation of v_3, which is believed to represent a very efficient channel for CO_2 dissociation. Nevertheless, this hypothesis found increasingly less support since it is practically difficult to realize. With this purpose, pulsed discharges have been proposed. Theoretically, the pulse and inter-pulse time modulation can help to selectively excite v_3 while maintaining T_g low, which is a pre-condition to sustain a consistent V-T non-equilibrium and drive the stepwise excitation up to the dissociation limit of CO_2. On the other hand, experiments have not yet evidenced any prominent vibrational excitation in pulsed discharges, and T_3-T_g non-equilibrium seems limited to t < 1 ms and T_g < 500 K.

In this study, we focused on validation of chemistry and gas heating dynamics in the ideal case of pure CO_2 using the single-pulse measurements performed by Klarenaar *et al*. [8]. In a multi-pulse situation, reaction products build up. Our present model needs to be expanded with an accurate description of CO, O and O_2 in order to assess their effect on chemistry and gas heating. Nevertheless, this study sets the stage for an in-depth and self-consistent investigation of the mechanisms underlying the energy exchanges in CO_2 low-temperature plasmas.

Thus far, modelling investigations focused on the study of the vibrational kinetics, identifying V-T relaxation as central mechanism for vibrational depopulation and gas heating. However, the energy transfer between different vibrational modes still lacks a clear interpretation. In particular, here we pinpoint the key role of V-V-T relaxation in coupling the kinetics of v_3 and v_{12}. The validation of our new kinetic scheme with experiments provides evidence of the essential contribution of v_{12} in promoting the gas heating in pure CO_2 discharges.

In addition, V-T relaxation alone cannot fully describe the heating dynamics under typical experimental conditions. This hypothesis was recently supported by some experimental and theoretical investigations [14,46], and finds confirmation in our study. In particular, our 0D simulations with self-consistent calculation of T_g predict a contribution of ca. 35 % to gas heating from electronic relaxation, and even up to nearly 100% during the onset of the discharge. Despite the uncertainties related to the characterization of the electronic states of CO_2 and the lack of accurate relaxation rates, our work strongly suggests the importance of electronic collisional quenching to portray the underlying heating mechanism in CO_2 plasmas. Finally, it is worth mentioning that the O atom kinetics plays an important role in the heating dynamics as well, becoming essential to describe the energy transfers in the afterglow, where the electron kinetics is quenched. This observation confirms the insights provided by previous studies on CO_2 low-pressure plasmas and will be subject of more in-depth investigation in a future publication. Indeed, we expect the role of V-T relaxation by O atoms in the heating dynamics to become even more important in discharges with higher dissociation degrees, i.e. in discharges in continuous regime.

This modelling effort establishes the basis for the redefinition of the operational parameter space for sustaining a consistent vibrational excitation and its potential contribution into CO_2 dissociation. The polyatomic nature of CO_2 and, therefore, the existence of low-lying symmetric stretching and bending levels besides the asymmetric levels is a major constraint to a strong V-T non-equilibrium. Additional limitation is posed by the fast loss of energy into electronic states and, subsequently, heat, which seems to be unavoidable in pulsed regimes. Moreover, the presence of dissociation products (e.g. O atoms, as demonstrated in this study) can alter the vibrational distribution and the heating dynamics during the active phase of the discharge and in

the afterglow. Therefore, in our future work we will prosecute the investigation and expand the study to experimental conditions where a non-negligible dissociation degree exists in the plasma.

Conflict of interest

There are no conflicts of interest to declare.

Acknowledgements

This research was supported by the European Union's Horizon 2020 Research and Innovation programme under the Marie Sklodowska-Curie grant agreement No 813393 (PIONEER). V. Guerra and T. Silva were partially funded by the Portuguese 'FCT-Fundação para a Ciência e a Tecnologia', under projects UIDB/50010/2020, UIDP/50010/2020, PTDC/FIS-PLA/1616/2021 and EXPL/FIS-PLA/0076/2021. The calculations were performed using the Turing HPC infrastructure at the CalcUA core facility of the Universiteit Antwerpen (UAntwerpen), a division of the Flemish Supercomputer Center VSC, funded by the Hercules Foundation, the Flemish Government (department EWI) and the UAntwerpen.

Data availability statement

The data that supports the findings of this study is available upon reasonable request from the authors.

ORCID iDs

O Biondo https://orcid.org/0000-0002-8061-4525

C Fromentin https://orcid.org/0000-0002-8230-2322

T Silva https://orcid.org/0000-0001-9046-958X

V Guerra https://orcid.org/0000-0002-6878-6850

G van Rooij https://orcid.org/0000-0003-4795-3274

A Bogaerts https://orcid.org/0000-0001-9875-6460

Appendix A. Chemistry set

Table A1. List of the 101 CO_2 vibrational states considered in this study, with the corresponding energies and statistical weights. Details on the notation used, as well as on the calculation of the vibrational energies, can be found in Section 2.

Vibrational state	Energy (eV)	Statistical weight
$CO_2(00^00 1)$	0.000000	1
$CO_2(01^10 1)$	0.082793	2
$CO_2(02^20 1)$	0.165728	2
$CO_2(10^00 2)$	0.165742	2
$CO_2(11^10 2)$	0.248597	4
$CO_2(03^30 1)$	0.248807	2
$CO_2(00^01 1)$	0.291257	1
$CO_2(20^00 3)$	0.331312	3
$CO_2(12^20 2)$	0.331593	4
$CO_2(04^40 1)$	0.332032	2
$CO_2(01^11 1)$	0.372499	2
$CO_2(21^10 3)$	0.414216	6
$CO_2(13^30 2)$	0.414733	4
$CO_2(05^50 1)$	0.415403	2
$CO_2(02^21 1)$	0.453883	2
$CO_2(10^01 2)$	0.454254	2
$CO_2(30^00 4)$	0.496695	4
$CO_2(22^20 3)$	0.497261	6
$CO_2(14^40 2)$	0.498018	4

$CO_2(06^601)$	0.498924	2
$CO_2(03^311)$	0.535413	2
$CO_2(11^112)$	0.535558	4
$CO_2(00^021)$	0.579419	1
$CO_2(31^104)$	0.579636	8
$CO_2(23^303)$	0.580449	6
$CO_2(15^502)$	0.581450	4
$CO_2(07^701)$	0.582590	2
$CO_2(12^212)$	0.617004	4
$CO_2(20^013)$	0.617074	3
$CO_2(04^411)$	0.617089	2
$CO_2(01^121)$	0.659113	2
$CO_2(13^312)$	0.698596	4
$CO_2(05^511)$	0.698914	2
$CO_2(21^113)$	0.699517	6
$CO_2(02^221)$	0.738951	2
$CO_2(10^022)$	0.739683	2
$CO_2(30^014)$	0.779701	4
$CO_2(22^213)$	0.779923	6
$CO_2(14^412)$	0.780333	4
$CO_2(06^611)$	0.780889	2
$CO_2(03^321)$	0.818936	2
$CO_2(11^122)$	0.819440	4
$CO_2(00^031)$	0.864490	1
$CO_2(04^421)$	0.899069	2
$CO_2(12^222)$	0.899341	4
$CO_2(20^023)$	0.899764	3
$CO_2(01^131)$	0.942641	2
$CO_2(05^521)$	0.979351	2
$CO_2(13^322)$	0.979388	4
$CO_2(21^123)$	0.979571	6
$CO_2(02^231)$	1.020937	2
$CO_2(10^032)$	1.022033	2
$CO_2(22^223)$	1.059523	6
$CO_2(14^422)$	1.059583	4
$CO_2(30^024)$	1.059647	4
$CO_2(06^621)$	1.059786	2
$CO_2(03^331)$	1.099382	2
$CO_2(11^132)$	1.100247	4
$CO_2(00^041)$	1.146474	1
$CO_2(12^232)$	1.177932	4
$CO_2(04^431)$	1.177976	2
$CO_2(20^033)$	1.179387	3
$CO_2(01^141)$	1.223087	2
$CO_2(05^531)$	1.256721	2

$CO_2(13^332)$	1.257116	4
$CO_2(21^133)$	1.257653	6
$CO_2(02^241)$	1.299846	2
$CO_2(10^042)$	1.301308	2
$CO_2(06^631)$	1.335618	2
$CO_2(14^432)$	1.335773	4
$CO_2(22^233)$	1.336065	6
$CO_2(30^034)$	1.336539	4
$CO_2(03^341)$	1.376755	2
$CO_2(11^142)$	1.377985	4
$CO_2(00^051)$	1.425377	1
$CO_2(04^441)$	1.453814	2
$CO_2(12^242)$	1.454809	4
$CO_2(20^043)$	1.455948	3
$CO_2(01^151)$	1.500456	2
$CO_2(05^541)$	1.531026	2
$CO_2(13^342)$	1.531782	4
$CO_2(21^143)$	1.532678	6
$CO_2(02^251)$	1.575683	2
$CO_2(10^052)$	1.577514	2
$CO_2(06^641)$	1.608392	2
$CO_2(14^442)$	1.608906	4
$CO_2(22^243)$	1.609554	6
$CO_2(30^044)$	1.610381	4
$CO_2(03^351)$	1.651060	2
$CO_2(11^152)$	1.652658	4
$CO_2(04^451)$	1.726590	2
$CO_2(12^252)$	1.727951	4
$CO_2(20^053)$	1.729453	3
$CO_2(05^551)$	1.802273	2
$CO_2(13^352)$	1.803393	4
$CO_2(21^153)$	1.804650	6
$CO_2(06^651)$	1.878112	2
$CO_2(14^452)$	1.878988	4
$CO_2(22^253)$	1.879995	6
$CO_2(30^054)$	1.881178	4

Table A2. Chemistry set proposed in this work. Rate coefficients in $cm^3\ s^{-1}$ or $cm^6\ s^{-1}$, for two-body and three-body reactions, respectively, while T_e in eV and T_g in K. Note that CO_2 represents the sum of all the CO_2 vibrational states considered in this study and no scaling laws were

applied to the rate coefficients to account for the vibrational energy of the reactants, unless specified differently (i.e. for electron-impact vibrational excitation and V-T, V-V-T and V-V reactions).

Reaction	Rate coefficients	Reference
e^- impact ionization/excitation/dissociation		
$e + CO_2 \rightarrow e + e + CO_2^+$	EEDF	[69]
$e + CO_2 \rightarrow e + CO + O(^1D)$	EEDF	[90]
$e + CO_2 \rightarrow e + CO(a^3\Pi) + O$	EEDF	[90]
$e + CO_2 \rightarrow e + CO_2(E1)$	EEDF (see section 3.4)	
$e + CO_2 \rightarrow e + CO_2(E2)$	EEDF (see section 3.4)	
$e + CO_2 \rightarrow e + CO_2(v_1v_2v_3)$	EEDF (see section 3.2)	
$e + CO \rightarrow e + e + CO^+$	EEDF	[69]
$e + CO \rightarrow e + C + O$	EEDF	[69]
$e + CO \rightarrow e + CO(a^3\Pi)$	EEDF	[69]
$e + O_2 \rightarrow e + e + O_2^+$	EEDF	[69]
$e + CO \rightarrow e + O + O$	EEDF	[69]
$e + CO \rightarrow e + O + O(^1D)$	EEDF	[69]
$e + O \rightarrow e + e + O^+$	EEDF	[69]
$e + O \rightarrow e + O(^1D)$	EEDF	[69]
e^- impact recombination or attachment/detachment		
$e + CO_2 \rightarrow CO + O^-$	EEDF	[69]
$e + CO \rightarrow C + O^-$	EEDF	[69]
$e + O_2 \rightarrow O + O^-$	EEDF	[69]
$e + CO_2^+ \rightarrow CO + O$		[101,102]
$e + CO_2^+ \rightarrow C + O_2$		[103]
$e + CO^+ \rightarrow C + O$		[104,105]
$e + O_2^+ + M \rightarrow O_2 + M$		[101]
$e + O_2^+ \rightarrow O + O$		[104]
$e + O + M \rightarrow O^- + M$		[106]
$e + O^- \rightarrow e + e + O$	EEDF	[69]
Ion-neutral and ion-ion reactions		
$CO_2^+ + O \rightarrow CO_2 + O^+$		[107]
$CO_3^- + O \rightarrow CO_2 + O_2^-$		[108]
$CO_4^- + O \rightarrow CO_3^- + O_2$		[109]
$O_2^- + O \rightarrow O_2 + O^-$		[109]
$O_2^+ + C \rightarrow CO^+ + O$		[107]
$CO_2^+ + O \rightarrow O_2^+ + CO$		[107]
$CO_2^+ + O_2 \rightarrow CO_2 + O_2^+$		[107]
$CO^+ + O_2 \rightarrow CO + O_2^+$		[107]
$O^+ + CO_2 \rightarrow O + CO_2^+$		[103]
$CO^+ + CO_2 \rightarrow CO + CO_2^+$		[109,110]
$O^+ + CO_2 \rightarrow O_2^+ + CO$		[103]
$O^+ + O^- \rightarrow O + O$		[111]
$O_2^+ + O^- \rightarrow O_2 + O$		[101]
$O_2^+ + O^- \rightarrow O + O + O$		[111]
$O_2^+ + O_2^- \rightarrow O_2 + O_2$		[111]
$O_2^+ + O_2^- \rightarrow O_2 + O + O$		[101]
$O_2^+ + O_2^- + M \rightarrow O_2 + O_2 + M$		[112]
$O_2^+ + CO_3^- \rightarrow CO + O_2 + O$		[101]
$O_2^+ + CO_4^- \rightarrow CO + O_2 + O_2$		[101]

$CO_2^+ + O_2^-$ $CO + O_2 + O$		[106]
$CO_2^+ + CO_3^-$ $CO_2(10002) + CO_2(10002) + O$		[106]
$CO_2^+ + CO_4^-$ $CO_2(10002) + CO_2(10002) + O_2$		[106]
$O^- + M$ $O + e + M$		[113–115]
$O_2^- + M$ $O_2 + e + M$		[116]
$O^- + O$ $O_2 + e$		[117]
$O^- + CO$ $CO_2 + e$		[118]
$O^- + CO_2 + CO_2$ $CO_3^- + CO_2$		[109,119]
$O^- + CO_2 + CO$ $CO_3^- + CO$		[109,119]
$O^- + CO_2 + O_2$ $CO_3^- + O_2$		[109,119]
$O_2^- + CO_2 + M$ $CO_4^- + M$		[109,119]
V-V, V-V-T and V-V reactions (see section 3.3)		
Neutral-neutral reactions		
$CO_2 + M$ $CO + O + M$		[120]
$CO_2 + O$ $CO + O_2$		[121]
$CO_2 + C$ $CO + CO$		[122]
$CO + M$ $C + O + M$		[123]
$O_2 + M$ $O + O + M$		[123]
$O_2 + CO$ $O + CO_2$		[124]
$CO + O + CO_2$ $CO_2 + CO_2$		[123,125]
$CO + O + CO$ $CO_2 + CO$		[123,125]
$CO + O + O_2$ $CO_2 + O_2$		[123,125]
$O + C + M$ $CO + M$		[123]
$O_2 + C + M$ $CO + O + M$		[126]
$O + O + M$ $O_2 + M$		[123]
$CO(a^3\Pi) + O_2$ $CO + O + O$		[127]
$CO(a^3\Pi) + CO$ $CO_2 + C$		[127]
$CO(a^3\Pi) + CO_2$ $CO + CO + O$		[128]
$CO + O(^1D)$ CO_2		[129]
Collisional quenching of electronic states		
$CO(a^3\Pi) + O$ $CO + O$		[130]
$CO(a^3\Pi) + O_2$ $CO + O_2$		[127]
$CO(a^3\Pi) + CO$ $CO + CO$		[127]
$CO(a^3\Pi) + CO_2$ $CO + CO_2$		[128]
$O(^1D) + O$ $O + O$		[131]
$O(^1D) + O_2$ $O + O_2$		[132]
$O(^1D) + CO$ $O + CO$		[133]
$O(^1D) + CO_2$ $O + CO_2$		[132]
$CO_2(E1) + M$ $CO_2 + M$	(see section 3.4)	
$CO_2(E1) + M$ $CO_2 + M$	(see section 3.4)	

References

[1] H.S. Baker, R.J. Millar, D.J. Karoly, U. Beyerle, B.P. Guillod, D. Mitchell, H. Shiogama, S. Sparrow, T. Woollings, M.R. Allen, Higher CO2 concentrations increase extreme event risk in a 1.5 °C world, Nat. Clim. Change. 8 (2018) 604–608. https://doi.org/10.1038/s41558-018-0190-1.

[2] M. Steinacher, F. Joos, T.F. Stocker, Allowable carbon emissions lowered by multiple climate targets, Nature. 499 (2013) 197–201. https://doi.org/10.1038/nature12269.

[3] S.I. Seneviratne, M.G. Donat, A.J. Pitman, R. Knutti, R.L. Wilby, Allowable CO2 emissions based on regional and impact-related climate targets, Nature. 529 (2016) 477–483. https://doi.org/10.1038/nature16542.
[4] D. Tong, Q. Zhang, Y. Zheng, K. Caldeira, C. Shearer, C. Hong, Y. Qin, S.J. Davis, Committed emissions from existing energy infrastructure jeopardize 1.5 °C climate target, Nature. 572 (2019) 373–377. https://doi.org/10.1038/s41586-019-1364-3.
[5] BP Statistical Review of World Energy, BP Statistical Review of World Energy, (2019). https://www.bp.com/content/dam/bp/business-sites/en/global/corporate/pdfs/energy-economics/statistical-review/bp-stats-review-2019-full-report.pdf (accessed March 21, 2022).
[6] G.J. van Rooij, H.N. Akse, W.A. Bongers, M.C.M. van de Sanden, Plasma for electrification of chemical industry: a case study on CO_2 reduction, Plasma Phys. Control. Fusion. 60 (2018) 014019. https://doi.org/10.1088/1361-6587/aa8f7d.
[7] A. Bogaerts, G. Centi, Plasma Technology for CO2 Conversion: A Personal Perspective on Prospects and Gaps, Front. Energy Res. 8 (2020) 111. https://doi.org/10.3389/fenrg.2020.00111.
[8] B.L.M. Klarenaar, R. Engeln, D.C.M. van den Bekerom, M.C.M. van de Sanden, A.S. Morillo-Candas, O. Guaitella, Time evolution of vibrational temperatures in a CO_2 glow discharge measured with infrared absorption spectroscopy, Plasma Sources Sci. Technol. 26 (2017) 115008. https://doi.org/10.1088/1361-6595/aa902e.
[9] T. Silva, M. Grofulović, B.L.M. Klarenaar, A.S. Morillo-Candas, O. Guaitella, R. Engeln, C.D. Pintassilgo, V. Guerra, Kinetic study of low-temperature CO_2 plasmas under non-equilibrium conditions. I. Relaxation of vibrational energy, Plasma Sources Sci. Technol. 27 (2018) 015019. https://doi.org/10.1088/1361-6595/aaa56a.
[10] G. Trenchev, A. Nikiforov, W. Wang, St. Kolev, A. Bogaerts, Atmospheric pressure glow discharge for CO2 conversion: Model-based exploration of the optimum reactor configuration, Chem. Eng. J. 362 (2019) 830–841. https://doi.org/10.1016/j.cej.2019.01.091.
[11] D.C.M. van den Bekerom, J.M.P. Linares, T. Verreycken, E.M. van Veldhuizen, S. Nijdam, G. Berden, W.A. Bongers, M.C.M. van de Sanden, G.J. van Rooij, The importance of thermal dissociation in CO_2 microwave discharges investigated by power pulsing and rotational Raman scattering, Plasma Sources Sci. Technol. 28 (2019) 055015. https://doi.org/10.1088/1361-6595/aaf519.
[12] G.J. van Rooij, D.C.M. van den Bekerom, N. den Harder, T. Minea, G. Berden, W.A. Bongers, R. Engeln, M.F. Graswinckel, E. Zoethout, M.C.M. van de Sanden, Taming microwave plasma to beat thermodynamics in CO_2 dissociation, Faraday Discuss. 183 (2015) 233–248. https://doi.org/10.1039/C5FD00045A.
[13] A. Vesel, M. Mozetic, A. Drenik, M. Balat-Pichelin, Dissociation of CO2 molecules in microwave plasma, Chem. Phys. 382 (2011) 127–131. https://doi.org/10.1016/j.chemphys.2011.03.015.
[14] A.W. van de Steeg, T. Butterworth, D.C.M. van den Bekerom, A.F. Silva, M.C.M. van de Sanden, G.J. van Rooij, Plasma activation of N_2, CH_4 and CO_2: an assessment of the vibrational non-equilibrium time window, Plasma Sources Sci. Technol. 29 (2020) 115001. https://doi.org/10.1088/1361-6595/abbae4.
[15] A.W. van de Steeg, L. Vialetto, A.F.S. da Silva, P. Viegas, P. Diomede, M.C.M. van de Sanden, G.J. van Rooij, The Chemical Origins of Plasma Contraction and Thermalization

in CO_2 Microwave Discharges, J. Phys. Chem. Lett. 13 (2022) 1203–1208. https://doi.org/10.1021/acs.jpclett.1c03731.
[16] L. Vialetto, A. van de Steeg, P. Viegas, S. Longo, G.J. Van Rooij, R. Van de Sanden, J. van Dijk, P. Diomede, Charged particle kinetics and gas heating in CO_2 microwave plasma contraction: comparisons of simulations and experiments, Plasma Sources Sci. Technol. (2022). https://doi.org/10.1088/1361-6595/ac56c5.
[17] V. Vermeiren, A. Bogaerts, Plasma-Based CO_2 Conversion: To Quench or Not to Quench?, J. Phys. Chem. C. 124 (2020) 18401–18415. https://doi.org/10.1021/acs.jpcc.0c04257.
[18] R. Snoeckx, A. Bogaerts, Plasma technology – a novel solution for CO_2 conversion?, Chem. Soc. Rev. 46 (2017) 5805–5863. https://doi.org/10.1039/C6CS00066E.
[19] N. den Harder, D.C.M. van den Bekerom, R.S. Al, M.F. Graswinckel, J.M. Palomares, F.J.J. Peeters, S. Ponduri, T. Minea, W.A. Bongers, M.C.M. van de Sanden, G.J. van Rooij, Homogeneous CO_2 conversion by microwave plasma: Wave propagation and diagnostics, Plasma Process. Polym. 14 (2017) 1600120. https://doi.org/10.1002/ppap.201600120.
[20] W. Bongers, H. Bouwmeester, B. Wolf, F. Peeters, S. Welzel, D. van den Bekerom, N. den Harder, A. Goede, M. Graswinckel, P.W. Groen, J. Kopecki, M. Leins, G. van Rooij, A. Schulz, M. Walker, R. van de Sanden, Plasma-driven dissociation of CO_2 for fuel synthesis, Plasma Process. Polym. 14 (2017) 1600126. https://doi.org/10.1002/ppap.201600126.
[21] Iu.P. Butylkin, V.K. Zhivotov, E.G. Krasheninnikov, M.F. Krotov, V.D. Rusanov, Iu.V. Tarasov, A.A. Fridman, Plasma-chemical process of CO2 dissociation in a nonequilibrium microwave discharge, Zhurnal Tekhnicheskoi Fiz. 51 (1981) 925–931.
[22] V.D. Rusanov, A.A. Fridman, G.V. Sholin, The physics of a chemically active plasma with nonequilibrium vibrational excitation of molecules, Sov. Phys. Uspekhi. 24 (1981) 447–474. https://doi.org/10.1070/PU1981v024n06ABEH004884.
[23] A. van de Steeg, P. Viegas, A. Silva, T. Butterworth, A. van Bavel, J. Smits, P. Diomede, M. van de Sanden, G. van Rooij, Redefining the Microwave Plasma-Mediated CO_2 Reduction Efficiency Limit: The Role of O–CO_2 Association, ACS Energy Lett. 6 (2021) 2876–2881. https://doi.org/10.1021/acsenergylett.1c01206.
[24] C.E. Treanor, Vibrational Energy Transfer in High-Energy Collisions, J. Chem. Phys. 43 (1965) 532–538. https://doi.org/10.1063/1.1696777.
[25] L. Chen, J.A. Lau, D. Schwarzer, J. Meyer, V.B. Verma, A.M. Wodtke, The Sommerfeld ground-wave limit for a molecule adsorbed at a surface, Science. 363 (2019) 158–161. https://doi.org/10.1126/science.aav4278.
[26] A. Fridman, Plasma Chemistry, Cambridge: Cambridge University Press, 2008.
[27] P. Capezzuto, F. Cramarossa, R. D'Agostino, E. Molinari, Contribution of vibrational excitation to the rate of carbon dioxide dissociation in electrical discharges, J. Phys. Chem. 80 (1976) 882–888. https://doi.org/10.1021/j100549a024.
[28] A. Bogaerts, T. Kozák, K. van Laer, R. Snoeckx, Plasma-based conversion of CO_2: current status and future challenges, Faraday Discuss. 183 (2015) 217–232. https://doi.org/10.1039/C5FD00053J.
[29] T. Kozák, A. Bogaerts, Splitting of CO_2 by vibrational excitation in non-equilibrium plasmas: a reaction kinetics model, Plasma Sources Sci. Technol. 23 (2014) 045004. https://doi.org/10.1088/0963-0252/23/4/045004.

[30] P. Diomede, M.C.M. van de Sanden, S. Longo, Insight into CO_2 Dissociation in Plasma from Numerical Solution of a Vibrational Diffusion Equation, J. Phys. Chem. C. 121 (2017) 19568–19576. https://doi.org/10.1021/acs.jpcc.7b04896.
[31] C.J.S.M. Simpson, K.B. Bridgman, T.R.D. Chandler, Shock-Tube Study of Vibrational Relaxation in Carbon Dioxide, J. Chem. Phys. 49 (1968) 513–522. https://doi.org/10.1063/1.1670105.
[32] V. Vermeiren, A. Bogaerts, Improving the Energy Efficiency of CO_2 Conversion in Nonequilibrium Plasmas through Pulsing, J. Phys. Chem. C. 123 (2019) 17650–17665. https://doi.org/10.1021/acs.jpcc.9b02362.
[33] T. Silva, M. Grofulović, L. Terraz, C.D. Pintassilgo, V. Guerra, Modelling the input and relaxation of vibrational energy in CO_2 plasmas, J. Phys. Appl. Phys. 51 (2018) 464001. https://doi.org/10.1088/1361-6463/aadbd7.
[34] M. Grofulović, T. Silva, B.L.M. Klarenaar, A.S. Morillo-Candas, O. Guaitella, R. Engeln, C.D. Pintassilgo, V. Guerra, Kinetic study of CO_2 plasmas under non-equilibrium conditions. II. Input of vibrational energy, Plasma Sources Sci. Technol. 27 (2018) 115009. https://doi.org/10.1088/1361-6595/aadb60.
[35] T. Silva, A.S. Morillo-Candas, O. Guaitella, V. Guerra, Modeling the time evolution of the dissociation fraction in low-pressure CO2 plasmas, J. CO2 Util. 53 (2021) 101719. https://doi.org/10.1016/j.jcou.2021.101719.
[36] V. Kotov, P.M.J. Koelman, Plug flow reactor model of the plasma chemical conversion of CO_2, Plasma Sources Sci. Technol. 28 (2019) 095002. https://doi.org/10.1088/1361-6595/ab3774.
[37] B.L.M. Klarenaar, M. Grofulović, A.S. Morillo-Candas, D.C.M. van den Bekerom, M.A. Damen, M.C.M. van de Sanden, O. Guaitella, R. Engeln, A rotational Raman study under non-thermal conditions in a pulsed CO_2 glow discharge, Plasma Sources Sci. Technol. 27 (2018) 045009. https://doi.org/10.1088/1361-6595/aabab6.
[38] L.M. Isola, B.J. Gómez, V. Guerra, Determination of the electron temperature and density in the negative glow of a nitrogen pulsed discharge using optical emission spectroscopy, J. Phys. Appl. Phys. 43 (2010) 015202. https://doi.org/10.1088/0022-3727/43/1/015202.
[39] J.P. Booth, O. Guaitella, A. Chatterjee, C. Drag, V. Guerra, D. Lopaev, S. Zyryanov, T. Rakhimova, D. Voloshin, Y. Mankelevich, Oxygen (^{3}P) atom recombination on a Pyrex surface in an O_2 plasma, Plasma Sources Sci. Technol. 28 (2019) 055005. https://doi.org/10.1088/1361-6595/ab13e8.
[40] M.L. da Silva, V. Guerra, J. Loureiro, Two-temperature models for nitrogen dissociation, Chem. Phys. 342 (2007) 275–287. https://doi.org/10.1016/j.chemphys.2007.10.010.
[41] A. Kosareva, O. Kunova, E. Kustova, E. Nagnibeda, Hybrid approach to accurate modeling of coupled vibrational-chemical kinetics in carbon dioxide, Phys. Fluids. 34 (2022) 026105. https://doi.org/10.1063/5.0079664.
[42] C.D. Pintassilgo, V. Guerra, Power Transfer to Gas Heating in Pure N_2 and in N_2–O_2 Plasmas, J. Phys. Chem. C. 120 (2016) 21184–21201. https://doi.org/10.1021/acs.jpcc.6b05463.
[43] S. Kelly, A. van de Steeg, A. Hughes, G. van Rooij, A. Bogaerts, Thermal instability and volume contraction in a pulsed microwave N_2 plasma at sub-atmospheric pressure, Plasma Sources Sci. Technol. 30 (2021) 055005. https://doi.org/10.1088/1361-6595/abf1d6.

[44] N.A. Popov, S.M. Starikovskaia, Relaxation of electronic excitation in nitrogen/oxygen and fuel/air mixtures: fast gas heating in plasma-assisted ignition and flame stabilization, Prog. Energy Combust. Sci. (2022) 100928. https://doi.org/10.1016/j.pecs.2021.100928.
[45] T. Silva, M. Grofulović, L. Terraz, C.D. Pintassilgo, V. Guerra, Dynamics of Gas Heating in the Afterglow of Pulsed CO2 and CO2–N2 Glow Discharges at Low Pressure, Plasma Chem. Plasma Process. 40 (2020) 713–725. https://doi.org/10.1007/s11090-020-10061-7.
[46] G.V. Pokrovskiy, N.A. Popov, S.M. Starikovskaia, Fast gas heating and kinetics of electronically excited states in a nanosecond capillary discharge in CO_2, Plasma Sources Sci. Technol. 31 (2022) 035010. https://doi.org/10.1088/1361-6595/ac5102.
[47] N.A. Popov, Investigation of the mechanism for rapid heating of nitrogen and air in gas discharges, Plasma Phys. Rep. 27 (2001) 886–896. https://doi.org/10.1134/1.1409722.
[48] N. Britun, T. Silva, G. Chen, T. Godfroid, J. van der Mullen, R. Snyders, Plasma-assisted CO_2 conversion: optimizing performance via microwave power modulation, J. Phys. Appl. Phys. 51 (2018) 144002. https://doi.org/10.1088/1361-6463/aab1ad.
[49] T. Kozák, A. Bogaerts, Evaluation of the energy efficiency of CO_2 conversion in microwave discharges using a reaction kinetics model, Plasma Sources Sci. Technol. 24 (2014) 015024. https://doi.org/10.1088/0963-0252/24/1/015024.
[50] A. Berthelot, A. Bogaerts, Modeling of CO_2 Splitting in a Microwave Plasma: How to Improve the Conversion and Energy Efficiency, J. Phys. Chem. C. 121 (2017) 8236–8251. https://doi.org/10.1021/acs.jpcc.6b12840.
[51] A. Berthelot, A. Bogaerts, Modeling of CO_2 plasma: effect of uncertainties in the plasma chemistry, Plasma Sources Sci. Technol. 26 (2017) 115002. https://doi.org/10.1088/1361-6595/aa8ffb.
[52] G. Herzberg, Molecular spectra and molecular structure. 2 Infrared and Raman spectra of polyatomic molecules, London: Van Nostrand, 1960.
[53] I. Suzuki, General anharmonic force constants of carbon dioxide, J. Mol. Spectrosc. 25 (1968) 479–500. https://doi.org/10.1016/S0022-2852(68)80018-9.
[54] A. Chedin, The carbon dioxide molecule, J. Mol. Spectrosc. 76 (1979) 430–491. https://doi.org/10.1016/0022-2852(79)90236-4.
[55] A.G. Csaszar, Anharmonic force field of carbon dioxide, J. Phys. Chem. 96 (1992) 7898–7904. https://doi.org/10.1021/j100199a015.
[56] J.M.L. Martin, P.R. Taylor, T.J. Lee, Accurate ab initio quartic force fields for the N2O and CO2 molecules, Chem. Phys. Lett. 205 (1993) 535–542. https://doi.org/10.1016/0009-2614(93)80009-E.
[57] C.-P. Courtoy, SPECTRES DE VIBRATION-ROTATION DE MOLECULES SIMPLES DIATOMIQUES OU POLYATOMIQUES AVEC LONG PARCOURS D'ABSORPTION: XII. LE SPECTRE DE $C^{12}O^{16}_2$ ENTRE 3500 ET 8000 CM^{-1} ET LES CONSTANTES MOLECULAIRES DE CETTE MOLECULE, Can. J. Phys. 35 (1957) 608–648. https://doi.org/10.1139/p57-068.
[58] G. Herzberg, Molecular spectra and molecular structure. 2 Infrared and Raman spectra of polyatomic molecules, New York: D Van Nostrand, 1945.
[59] J. Blauer, G. Nickerson, A survey of vibrational relaxation rate data for processes importantto CO2-N2-H2O infrared plume radiation, in: 7th Fluid PlasmaDynamics Conf., American Institute of Aeronautics and Astronautics, Palo Alto,CA,U.S.A., 1974. https://doi.org/10.2514/6.1974-536.

[60] P.W. Atkins, R. Friedman, Molecular Quantum Mechanics, New York: Oxford University Press, 2005.
[61] V. Joly, A. Roblin, Vibrational relaxation of CO2 (m, nl, p) in a CO2-N2 mixture. Part 1: Survey of available data, Aerosp. Sci. Technol. 3 (1999) 229–238. https://doi.org/10.1016/S1270-9638(99)80045-5.
[62] D.M. Dennison, The Infra-Red Spectra of Polyatomic Molecules. Part II, Rev. Mod. Phys. 12 (1940) 175–214. https://doi.org/10.1103/RevModPhys.12.175.
[63] G. Amat, M. Pimbert, On Fermi resonance in carbon dioxide, J. Mol. Spectrosc. 16 (1965) 278–290. https://doi.org/10.1016/0022-2852(65)90123-2.
[64] D.C.M. van den Bekerom, A. van de Steeg, M.C.M. van de Sanden, G.J. van Rooij, Mode resolved heating dynamics in pulsed microwave CO_2 plasma from laser Raman scattering, J. Phys. Appl. Phys. 53 (2020) 054002. https://doi.org/10.1088/1361-6463/ab5311.
[65] A. Tejero-del-Caz, V. Guerra, D. Gonçalves, M.L. da Silva, L. Marques, N. Pinhão, C.D. Pintassilgo, L.L. Alves, The LisbOn KInetics Boltzmann solver, Plasma Sources Sci. Technol. 28 (2019) 043001. https://doi.org/10.1088/1361-6595/ab0537.
[66] The LisbOn KInetics (LoKI) 2020 http://plasmakit.tecnico. ulisboa.pt, (n.d.).
[67] S. Pancheshnyi, B. Eismann, G.J.M. Hagelaar, L.C. Pitchford, ZDPlasKin, (2008). http://www.zdplaskin.laplace.univ-tlse.fr.
[68] G.J.M. Hagelaar, L.C. Pitchford, Solving the Boltzmann equation to obtain electron transport coefficients and rate coefficients for fluid models, Plasma Sources Sci. Technol. 14 (2005) 722–733. https://doi.org/10.1088/0963-0252/14/4/011.
[69] M. Grofulović, L.L. Alves, V. Guerra, Electron-neutral scattering cross sections for CO_2: a complete and consistent set and an assessment of dissociation, J. Phys. Appl. Phys. 49 (2016) 395207. https://doi.org/10.1088/0022-3727/49/39/395207.
[70] M. Capitelli, ed., Plasma kinetics in atmospheric gases, Springer, Berlin ; New York, 2000.
[71] G.D. Billing, Vibration-Vibration and Vibration-Translation Energy Transfer, Including Multiquantum Transitions in Atom-Diatom and Diatom-Diatom Collisions, in: M. Capitelli (Ed.), Nonequilibrium Vib. Kinet., Springer Berlin Heidelberg, Berlin, Heidelberg, 1986: pp. 85–112. https://doi.org/10.1007/978-3-642-48615-9_4.
[72] R.N. Schwartz, Z.I. Slawsky, K.F. Herzfeld, Calculation of Vibrational Relaxation Times in Gases, J. Chem. Phys. 20 (1952) 1591–1599. https://doi.org/10.1063/1.1700221.
[73] D. Rapp, P. Englander-Golden, Resonant and Near-Resonant Vibrational—Vibrational Energy Transfer between Molecules in Collisions, J. Chem. Phys. 40 (1964) 573–575. https://doi.org/10.1063/1.1725158.
[74] R.D. Sharma, C.A. Brau, Energy Transfer in Near-Resonant Molecular Collisions due to Long-Range Forces with Application to Transfer of Vibrational Energy from ν3 Mode of CO_2 to N_2, J. Chem. Phys. 50 (1969) 924–930. https://doi.org/10.1063/1.1671145.
[75] A. Zelechow, D. Rapp, T.E. Sharp, Vibrational–Vibrational–Translational Energy Transfer between Two Diatomic Molecules, J. Chem. Phys. 49 (1968) 286–299. https://doi.org/10.1063/1.1669823.
[76] I.V. Adamovich, S.O. Macheret, J.W. Rich, C.E. Treanor, Vibrational Energy Transfer Rates Using a Forced Harmonic Oscillator Model, J. Thermophys. Heat Transf. 12 (1998) 57–65. https://doi.org/10.2514/2.6302.
[77] L.D. Pietanza, O. Guaitella, V. Aquilanti, I. Armenise, A. Bogaerts, M. Capitelli, G. Colonna, V. Guerra, R. Engeln, E. Kustova, A. Lombardi, F. Palazzetti, T. Silva,

Advances in non-equilibrium $$\hbox {CO}_2$$ plasma kinetics: a theoretical and experimental review, Eur. Phys. J. D. 75 (2021) 237. https://doi.org/10.1140/epjd/s10053-021-00226-0.
[78] A. Lagan, A. Lombardi, F. Pirani, P. Gamallo, R. Say s, I. Armenise, M. Cacciatore, F. Esposito, M. Rutigliano, Molecular Physics of Elementary Processes Relevant to Hypersonics: Atom-Molecule, Molecule-Molecule and Atoms-Surface Processes, Open Plasma Phys. J. 7 (2014) 48–59. https://doi.org/10.2174/1876534301407010048.
[79] A. Lombardi, N. Faginas-Lago, L. Pacifici, G. Grossi, Energy transfer upon collision of selectively excited CO_2 molecules: State-to-state cross sections and probabilities for modeling of atmospheres and gaseous flows, J. Chem. Phys. 143 (2015) 034307. https://doi.org/10.1063/1.4926880.
[80] W.Q. Jeffers, J.D. Kelley, Calculations of V–V Transfer Probabilities in CO–CO Collisions, J. Chem. Phys. 55 (1971) 4433–4437. https://doi.org/10.1063/1.1676770.
[81] R.T. Pack, Analytic estimation of almost resonant molecular energy transfer due to multipolar potentials. *V V* processes involving CO_2, J. Chem. Phys. 72 (1980) 6140–6152. https://doi.org/10.1063/1.439071.
[82] F. Lepoutre, G. Louis, H. Manceau, Collisional relaxation in CO2 between 180 K and 400 K measured by the spectrophone method, Chem. Phys. Lett. 48 (1977) 509–514. https://doi.org/10.1016/0009-2614(77)85082-3.
[83] M. López-Puertas, R. Rodrigo, A. Molina, F.W. Taylor, A non-LTE radiative transfer model for infrared bands in the middle atmosphere. I. Theoretical basis and application to CO2 15 μm bands, J. Atmospheric Terr. Phys. 48 (1986) 729–748. https://doi.org/10.1016/0021-9169(86)90022-X.
[84] M. Huetz-Aubert, F. Lepoutre, An optic-acoustic study of thermal vibrational relaxation in CO2 and in mixtures of CO2 with monoatomic gases, Physica. 78 (1974) 435–456. https://doi.org/10.1016/0031-8914(74)90373-5.
[85] M. Lopez-puertas, F.W. Taylor, Non-lte Radiative Transfer In The Atmosphere, World Scientific Publishing Company, 2001. https://books.google.be/books?id=NAvVCgAAQBAJ.
[86] L. Terraz, T. Silva, A. Morillo-Candas, O. Guaitella, A. Tejero-del-Caz, L.L. Alves, V. Guerra, Influence of N_2 on the CO_2 vibrational distribution function and dissociation yield in non-equilibrium plasmas, J. Phys. Appl. Phys. 53 (2020) 094002. https://doi.org/10.1088/1361-6463/ab55fb.
[87] A.S. Morillo-Candas, B.L.M. Klarenaar, C. Amoedo, V. Guerra, O. Guaitella, Effect of oxygen atoms on the vibrational kinetics of CO_2 and CO revealed by the use of a large surface area material, J. Phys. Appl. Phys. 54 (2021) 095208. https://doi.org/10.1088/1361-6463/abc992.
[88] J.J. Lowke, A.V. Phelps, B.W. Irwin, Predicted electron transport coefficients and operating characteristics of CO_2–N_2–He laser mixtures, J. Appl. Phys. 44 (1973) 4664–4671. https://doi.org/10.1063/1.1662017.
[89] N.Y. Babaeva, G.V. Naidis, On the efficiency of CO_2 conversion in corona and dielectric-barrier discharges, Plasma Sources Sci. Technol. 30 (2021) 03LT03. https://doi.org/10.1088/1361-6595/abe6e6.
[90] L.S. Polak, D.I. Slovetsky, Electron impact induced electronic excitation and molecular dissociation, Int. J. Radiat. Phys. Chem. 8 (1976) 257–282. https://doi.org/10.1016/0020-7055(76)90070-X.

[91] A. Bogaerts, W. Wang, A. Berthelot, V. Guerra, Modeling plasma-based CO_2 conversion: crucial role of the dissociation cross section, Plasma Sources Sci. Technol. 25 (2016) 055016. https://doi.org/10.1088/0963-0252/25/5/055016.
[92] A.S. Morillo-Candas, T. Silva, B.L.M. Klarenaar, M. Grofulović, V. Guerra, O. Guaitella, Electron impact dissociation of CO_2, Plasma Sources Sci. Technol. 29 (2020) 01LT01. https://doi.org/10.1088/1361-6595/ab6075.
[93] A.F. Silva, A.S. Morillo-Candás, A. Tejero-del-Caz, L.L. Alves, O. Guaitella, V. Guerra, A reaction mechanism for vibrationally-cold low-pressure CO_2 plasmas, Plasma Sources Sci. Technol. 29 (2020) 125020. https://doi.org/10.1088/1361-6595/abc818.
[94] V. Vesovic, W.A. Wakeham, G.A. Olchowy, J.V. Sengers, J.T.R. Watson, J. Millat, The Transport Properties of Carbon Dioxide, J. Phys. Chem. Ref. Data. 19 (1990) 763–808. https://doi.org/10.1063/1.555875.
[95] M. Chase Jr, NIST-JANAF thermochemical tables, J. Phys. Chem. Ref. Data Monograph. 9 (1998).
[96] J.L. Moruzzi, D.A. Price, Ionization, attachment and detachment in air and air-CO2 mixtures, J. Phys. Appl. Phys. 7 (1974) 1434–1440. https://doi.org/10.1088/0022-3727/7/10/317.
[97] W. Roznerski, K. Leja, Electron drift velocity in hydrogen, nitrogen, oxygen, carbon monoxide, carbon dioxide and air at moderate E/N, J. Phys. Appl. Phys. 17 (1984) 279–285. https://doi.org/10.1088/0022-3727/17/2/012.
[98] A.F. Silva, A.S. Morillo-Candás, A. Tejero-del-Caz, L.L. Alves, O. Guaitella, V. Guerra, A reaction mechanism for vibrationally-cold low-pressure CO2 plasmas, Plasma Sources Sci Technol. (2021) 17.
[99] M.A. Damen, L.M. Martini, R. Engeln, Temperature evolution in a pulsed CO_2–N_2 glow discharge measured using quantum cascade laser absorption spectroscopy, Plasma Sources Sci. Technol. 29 (2020) 065016. https://doi.org/10.1088/1361-6595/ab8e50.
[100] I. Armenise, E. Kustova, Mechanisms of Coupled Vibrational Relaxation and Dissociation in Carbon Dioxide, J. Phys. Chem. A. 122 (2018) 5107–5120. https://doi.org/10.1021/acs.jpca.8b03266.
[101] H. Hokazono, H. Fujimoto, Theoretical analysis of the CO_2 molecule decomposition and contaminants yield in transversely excited atmospheric CO_2 laser discharge, J. Appl. Phys. 62 (1987) 1585–1594. https://doi.org/10.1063/1.339606.
[102] R.E. Beverly, Ion aging effects on the dissociative-attachment instability in CO2 lasers, Opt. Quantum Electron. 14 (1982) 501–513. https://doi.org/10.1007/BF00610306.
[103] T.G. Beuthe, J.-S. Chang, Chemical Kinetic Modelling of Non-Equilibrium Ar-CO_2 Thermal Plasmas, Jpn. J. Appl. Phys. 36 (1997) 4997–5002. https://doi.org/10.1143/JJAP.36.4997.
[104] J.B.A. Mitchell, H. Hus, The dissociative recombination and excitation of CO^+, J. Phys. B At. Mol. Phys. 18 (1985) 547–555. https://doi.org/10.1088/0022-3700/18/3/029.
[105] D. McElroy, C. Walsh, A.J. Markwick, M.A. Cordiner, K. Smith, T.J. Millar, The UMIST database for astrochemistry 2012, Astron. Astrophys. 550 (2013) A36. https://doi.org/10.1051/0004-6361/201220465.
[106] J. Thoenes, S.C. Kurzius, Plasma Chemistry Processes in the Closed Cycle EDL., 1979. https://apps.dtic.mil/sti/citations/ADA083222.

[107] J. Woodall, M. Agúndez, A.J. Markwick-Kemper, T.J. Millar, The UMIST database for astrochemistry 2006, Astron. Astrophys. 466 (2007) 1197–1204. https://doi.org/10.1051/0004-6361:20064981.
[108] F.C. Fehsenfeld, A.L. Schmeltekopf, H.I. Schiff, E.E. Ferguson, Laboratory measurements of negative ion reactions of atmospheric interest, Planet. Space Sci. 15 (1967) 373–379. https://doi.org/10.1016/0032-0633(67)90201-2.
[109] D.L. Albritton, Ion-neutral reaction-rate constants measured in flow reactors through 1977, At. Data Nucl. Data Tables. 22 (1978) 1–89. https://doi.org/10.1016/0092-640X(78)90027-X.
[110] N.G. Adams, D. Smith, D. Grief, Reactions of HnCO+ ions with molecules at 300 K, Int. J. Mass Spectrom. Ion Phys. 26 (1978) 405–415. https://doi.org/10.1016/0020-7381(78)80059-X.
[111] J.T. Gudmundsson, E.G. Thorsteinsson, Oxygen discharges diluted with argon: dissociation processes, Plasma Sources Sci. Technol. 16 (2007) 399–412. https://doi.org/10.1088/0963-0252/16/2/025.
[112] B. Eliasson, M. Hirth, U. Kogelschatz, Ozone synthesis from oxygen in dielectric barrier discharges, J. Phys. Appl. Phys. 20 (1987) 1421–1437. https://doi.org/10.1088/0022-3727/20/11/010.
[113] M.H. Bortner, T. Baurer, Defense Nuclear Agency Reaction Rate Handbook, Second Edition, 1972. https://apps.dtic.mil/sti/citations/AD0763699.
[114] J.B. Hasted, R.A. Smith, The detachment of electrons from negative ions, Proc. R. Soc. Lond. Ser. Math. Phys. Sci. 235 (1956) 349–353. https://doi.org/10.1098/rspa.1956.0087.
[115] L. Frommhold, Über verzögerte Elektronen in Elektronenlawinen, insbesondere in Sauerstoff und Luft, durch Bildung und Zerfall negativer Ionen (O−), Fortschritte Phys. 12 (1964) 597–642. https://doi.org/10.1002/prop.19640121102.
[116] J.L. Pack, A.V. Phelps, Electron Attachment and Detachment. I. Pure O_2 at Low Energy, J. Chem. Phys. 44 (1966) 1870–1883. https://doi.org/10.1063/1.1726956.
[117] S.G. Belostotsky, D.J. Economou, D.V. Lopaev, T.V. Rakhimova, Negative ion destruction by O(^{3}P) atoms and O_2 ($a\,^1\Delta_g$) molecules in an oxygen plasma, Plasma Sources Sci. Technol. 14 (2005) 532–542. https://doi.org/10.1088/0963-0252/14/3/016.
[118] M. McFarland, D.L. Albritton, F.C. Fehsenfeld, E.E. Ferguson, A.L. Schmeltekopf, Flow-drift technique for ion mobility and ion-molecule reaction rate constant measurements. III. Negative ion reactions of O^- with CO, NO, H_2, and D_2, J. Chem. Phys. 59 (1973) 6629–6635. https://doi.org/10.1063/1.1680043.
[119] F.C. Fehsenfeld, E.E. Ferguson, Laboratory studies of negative ion reactions with atmospheric trace constituents, J. Chem. Phys. 61 (1974) 3181–3193. https://doi.org/10.1063/1.1682474.
[120] A. Eremin, V. Ziborov, V. Shumova, D. Voiki, P. Roth, Formation of O(1D) atoms in thermal decomposition of CO2, Kinet. Catal. 38 (1997) 1–7.
[121] S.C. Baber, A.M. Dean, Reaction of atomic oxygen with carbon dioxide behind reflected shock waves, J. Chem. Phys. 60 (1974) 307–313. https://doi.org/10.1063/1.1680785.
[122] A. Cenian, A. Chernukho, V. Borodin, Modeling of Plasma-Chemical Reactions in Gas Mixture of CO2 lasers. II. Theoretical Model and its Verification, Contrib. Plasma Phys. 35 (1995) 273–296. https://doi.org/10.1002/ctpp.2150350309.

[123] W. Tsang, R.F. Hampson, Chemical Kinetic Data Base for Combustion Chemistry. Part I. Methane and Related Compounds, J. Phys. Chem. Ref. Data. 15 (1986) 1087–1279. https://doi.org/10.1063/1.555759.
[124] L. Drummond, Shock-initiated exothermic reactions. IV. The oxidation of carbon monoxide, Aust. J. Chem. 21 (1968) 2631. https://doi.org/10.1071/CH9682631.
[125] R.R. Baldwin, D. Jackson, A. Melvin, B.N. Rossiter, The second limit of hydrogen + carbon monoxide + oxygen mixtures, Int. J. Chem. Kinet. 4 (1972) 277–292. https://doi.org/10.1002/kin.550040305.
[126] A.J. Dean, D.F. Davidson, R.K. Hanson, A shock tube study of reactions of carbon atoms with hydrogen and oxygen using excimer photolysis of C3O2 and carbon atom atomic resonance absorption spectroscopy, J. Phys. Chem. 95 (1991) 183–191. https://doi.org/10.1021/j100154a037.
[127] I.J. Wysong, Measurement of quenching rates of CO(a3Π,v=0) using laser pump-and-probe technique, Chem. Phys. Lett. 329 (2000) 42–46. https://doi.org/10.1016/S0009-2614(00)00967-2.
[128] M.P. Skrzypkowski, T. Gougousi, R. Johnsen, M.F. Golde, Measurement of the absolute yield of CO(a 3Π)+O products in the dissociative recombination of CO2+ ions with electrons, J. Chem. Phys. 108 (1998) 8400–8407. https://doi.org/10.1063/1.476267.
[129] J.C. Tully, Reactions of O(^1D) with atmospheric molecules, J. Chem. Phys. 62 (1975) 1893–1898. https://doi.org/10.1063/1.430675.
[130] W. Felder, W. Morrow, R.A. Young, CO(a3Π): rate coefficients for quenching by O(3P), Chem. Phys. Lett. 15 (1972) 100–103. https://doi.org/10.1016/0009-2614(72)87026-X.
[131] V.J. Abreu, J.H. Yee, S.C. Solomon, A. Dalgarno, The quenching rate of O(1D) by O(3P), Planet. Space Sci. 34 (1986) 1143–1145. https://doi.org/10.1016/0032-0633(86)90026-7.
[132] E.J. Dunlea, A.R. Ravishankara, Kinetic studies of the reactions of O(1D) with several atmospheric molecules, Phys. Chem. Chem. Phys. 6 (2004) 2152. https://doi.org/10.1039/b400247d.
[133] J.A. Davidson, H.I. Schiff, T.J. Brown, C.J. Howard, Temperature dependence of the deactivation of O(1D) by CO from 113–333 K, J. Chem. Phys. 69 (1978) 1216. https://doi.org/10.1063/1.436657.